Space - scale resolved surface-atmospheric fluxes across a heterogeneous, mid-latitude forested landscape

Sreenath Paleri[1], Ankur Rashmikant Desai[1], Stefan Metzger[2], David Durden[3], Brian Butterworth[4], Matthias R. Mauder[5], Katrin Kohnert[6], and Andrei Serafimovich[7]

[1]University of Wisconsin-Madison
[2]NEON Program, Battelle
[3]Battelle Ecology Inc.
[4]University of Colorado Boulder
[5]KIT
[6]German Council of Experts on Climate Change, Berlin, Germany
[7]GFZ German Research Centre for Geosciences, Telegrafenberg, Potsdam, Germany

November 30, 2022

Abstract

The Earth's surface is heterogeneous at multiple scales owing to spatial variability in various properties. The atmospheric responses to these heterogeneities through fluxes of energy, water, carbon and other scalars are scale-dependent and non-linear. Although these exchanges can be measured using the eddy covariance technique, widely used tower-based measurement approaches suffer from spectral losses in lower frequencies when using typical averaging times. However, spatially resolved measurements such as airborne eddy covariance measurements can detect such larger scale (meso-{β}, γ) transport. To evaluate the prevalence and magnitude of these flux contributions we applied wavelet analysis to airborne flux measurements over a heterogeneous mid-latitude forested landscape, interspersed with open water bodies and wetlands. The measurements were made during the Chequamegon Heterogeneous Ecosystem Energy-balance Study Enabled by a High-density Extensive Array of Detectors (CHEESEHEAD19) intensive field campaign. We ask, how do spatial scales of surface-atmosphere fluxes vary over heterogeneous surfaces across the day and across seasons? Measured fluxes were separated into smaller-scale turbulent and larger-scale mesoscale contributions. We found significant mesoscale contributions to H and LE fluxes through summer to autumn which wouldn't be resolved in single point tower measurements through traditional time-domain half-hourly Reynolds decomposition. We report scale-resolved flux transitions associated with seasonal and diurnal changes of the heterogeneous study domain. This study adds to our understanding of surface atmospheric interactions over unstructured heterogeneities and can help inform multi-scale model-data integration of weather and climate models at a sub-grid scale.

Space - scale resolved surface-atmospheric fluxes across a heterogeneous, mid-latitude forested landscape

Sreenath Paleri [1], Ankur R. Desai [1], Stefan Metzger [2,1], David Durden [2], Brian J. Butterworth [3,4], Matthias Mauder [5,6], Katrin Kohnert [7*], Andrei Serafimovich [7†]

[1]Department of Atmospheric and Oceanic Sciences, University of Wisconsin-Madison, Madison, Wisconsin, USA
[2]Battelle, National Ecological Observatory Network, 1685 38th Street, Boulder, Colorado, USA
[3]Cooperative Institute for Research in Environmental Sciences, University of Colorado, Boulder, Colorado, USA
[4]NOAA Physical Sciences Laboratory, Boulder, Colorado, USA
[5]Institute of Hydrology and Meteorology, Technische Universität Dresden, Dresden, Germany
[6]Institute of Meteorology and Climate Research – Atmospheric Environmental Research, Karlsruhe Institute of Technology, Garmisch-Partenkirchen, Germany
[7] GFZ German Research Centre for Geosciences, Telegrafenberg, Potsdam, Germany

Key Points:

- Substantial mesoscale surface atmospheric fluxes were measured across a heterogeneous mid latitude forested domain from a wavelet based analysis of airborne flux measurements.
- Measured fluxes show distinct seasonal and diurnal variations.
- Measured mesoscale fractions of sensible and latent heat fluxes do not behave similarly.

*Now at: German Council of Experts on Climate Change, Berlin, Germany
†Now at: Deutscher Wetterdienst, Offenbach, Germany

Corresponding author: Sreenath Paleri, paleri@wisc.edu

Abstract

The Earth's surface is heterogeneous at multiple scales owing to spatial variability in various properties. The atmospheric responses to these heterogeneities through fluxes of energy, water, carbon and other scalars are scale-dependent and non-linear. Although these exchanges can be measured using the eddy covariance technique, widely used tower-based measurement approaches suffer from spectral losses in lower frequencies when using typical averaging times. However, spatially resolved measurements such as airborne eddy covariance measurements can detect such larger scale (meso-β, γ) transport. To evaluate the prevalence and magnitude of these flux contributions we applied wavelet analysis to airborne flux measurements over a heterogeneous mid-latitude forested landscape, interspersed with open water bodies and wetlands. The measurements were made during the Chequamegon Heterogeneous Ecosystem Energy-balance Study Enabled by a High-density Extensive Array of Detectors (CHEESEHEAD19) intensive field campaign. We ask, how do spatial scales of surface-atmosphere fluxes vary over heterogeneous surfaces across the day and across seasons? Measured fluxes were separated into smaller-scale turbulent and larger-scale mesoscale contributions. We found significant mesoscale contributions to H and LE fluxes through summer to autumn which wouldn't be resolved in single point tower measurements through traditional time-domain half-hourly Reynolds decomposition. We report scale-resolved flux transitions associated with seasonal and diurnal changes of the heterogeneous study domain. This study adds to our understanding of surface atmospheric interactions over unstructured heterogeneities and can help inform multi-scale model-data integration of weather and climate models at a sub-grid scale.

Plain Language Summary

Accurate and reliable knowledge of the surface-atmospheric transport of mass and energy is essential to inform our theories and models of Earth system processes. Conventionally, such transport has been measured by tower mounted weather instruments that make high frequency measurements. However, experimental and simulation studies over the last couple of decades have shown that there is an imbalance between incoming, available energy and outgoing transport as observed from tower-mounted setups. A dominant hypothesis addressing this imbalance issue postulates that there exists significant larger landscape transport (of the order of 10-100 kms) over the course of a day. Single point tower measurements would not be able in include such transports in their conventional process flows. We use airborne data collected over a mid-latitude temperate forest in Northern-Wisconsin, USA to quantify large scale transport over the forested domain. Observations were made over the course of single days in July, August and September to include seasonal landscape transitions. The measured surface-atmospheric exchange is resolved into smaller and larger scale contributions using a space-frequency analysis framework that has been in use for aircraft measured atmospheric data. We report substantial large scale contributions with daily, seasonal and spatial characteristics.

1 Introduction

Surface atmospheric fluxes of energy, momentum, water, carbon and other scalars are integral components of Earth system processes. Terrestrial ecosystems act as important intermediaries for these exchange processes, influencing Earth's weather and climate systems (Pielke et al., 1998). However, the land surface is heterogeneous at multiple scales owing to spatial variability in multiple properties and the atmospheric responses to these heterogeneous surface forcings through the fluxes of energy, water, carbon and other scalars are also scale dependent and non-linear (Avissar & Schmidt, 1998). Since the scales of transport vary from Kolmogrov microscale in the turbulent regime to the mesoscale it is not easy to resolve the contributions from all of the relevant scales directly using observations or simulations (Bou-Zeid et al., 2020)

The primary transport process in the ABL is turbulence and the surface atmospheric turbulent fluxes can be directly measured using the eddy-covariance (EC) technique (Aubinet et al., 2012; Foken, 2017). The EC technique uses Reynold's decomposition of the Navier Stokes equation for momentum and scalar transport, with the assumptions of stationarity and horizontal homogeneity, to calculate turbulent fluxes in the atmospheric boundary layer (ABL). Tower based EC measurements are widely used to study ecosystem level biosphere-atmosphere interactions and quantify surface-atmospheric fluxes (Aubinet et al., 1999; Baldocchi et al., 2001). Even with careful experimental design and quality control, they are however limited by their surface flux footprints (i.e., part of the upstream surface contributing to the measured flux). Moreover, requirements for stationarity can complicate sampling flux contributions from lower frequencies as well (Desjardins et al., 1997; Mahrt, 2010)

So, a good first order sanity check on tower measured turbulent fluxes would be to check for the closure of the measured surface energy budget, evaluating whether available energy (the difference between measured net radiation and ground heat flux) within the control volume sampled by the tower is balanced by the measured sum of turbulent sensible and latent heat fluxes (Oncley et al., 2007; Foken, 2008; Foken et al., 2010; Mauder et al., 2020). Such a check would also be important to validate land surface and biological model parameters such as surface flux parameterisations in weather and climate models, water vapor surface conductances in ecosystem and land surface models or validating model predictions of net ecosystem exchanges (NEE). However, a persistent surface energy balance residual has been reported in prior investigations across multiple sites in multiple ecosystems (Oncley et al., 2007; Foken et al., 2010; Mauder et al., 2020)

Simulations and observational studies have shown that there can be larger scale transport linked to landscape variability. Based on their analysis of tower measured EC data Bernhofer (1992) had attributed the residuals to large scale non-turbulent transport driven by surface gradients. Finnigan et al. (2003) pointed out that the conventionally-used averaging windows of 30 minutes could act as a high pass filter for the data. They also noted that pre-treating tower measured turbulent data by rotating the measurement coordinates so that x-axis of measurement is aligned with the mean horizontal wind could also contribute to the same. Such data processing would remove contributions of motions with periods longer than the averaging times to the covariance being measured. Early Large Eddy Simulation (LES) studies (Kanda et al., 2004; Inagaki et al., 2006; Steinfeld et al., 2007) with idealized surface forcings indicated that transport due to turbulent organized structures and thermally-induced mesoscale structures can cause systematic underestimation of fixed point tower flux measurements. Maronga and Raasch (2013) conducted a LES study using measured sensible and latent heat fluxes as imposed surface boundary conditions over the LITFASS-2003 field experiment domain and diagnosed signals of heterogeneity-induced vertical velocities linked to landscape heterogeneities. Using a wavelet analysis of airborne turbulent data during the BOREAS field experiment, Mauder, Desjardins, and MacPherson (2008) quantified the mesoscale transport across a temperate heterogeneous landscape to be 10% of surface measured available energy and of the same order of magnitude as tower measured residuals over the domain. The LES study by K. Xu et al. (2020) employed simulated towers over idealized heterogeneities. Following a spatio-temporal eddy covariance approach for simulated towers they could account for 95% of the available energy with one tower per 40 km^2. Such a spatial approach seems to account for the landscape-scale low frequency transport. The recent LES study by (Margairaz et al., 2020) over idealized heterogeneities also shows that fluxes by secondary circulations can account for 5-10% of near surface sensible heat fluxes.

These investigations indicate that when surface heterogeneity starts influencing the surface-atmospheric transport, there can be quasi-stationary circulations modulated by the heterogeneity amplitudes and background wind. Such structures could lead to increased advective transport and flux divergences, thereby reducing the net transport associated with the turbulent covariance term, measured through the eddy covariance method (Mahrt, 2010;

Mauder et al., 2020). Quantifying and diagnosing such a 3 dimensional transport and horizontal variability of surface atmospheric fluxes over heterogeneous domains in the field calls for the deployment of intensive instrumentation that can sample the surface atmospheric exchanges at multiple, overlapping scales (Wulfmeyer et al., 2018). Identification and measurement of such structures and their contributions from field observations call for spatially resolving measurement techniques, such as a distributed tower network (Oncley et al., 2007; Mauder, Desjardins, Pattey, et al., 2008; Engelmann & Bernhofer, 2016; Morrison et al., 2021), airborne measurements (Mahrt, 1998; Strunin & Hiyama, 2004; Bange et al., 2002, 2006; Mauder, Oncley, et al., 2007), scintillometers (Foken et al., 2010; F. Xu et al., 2017; Meijninger et al., 2006) and LiDAR measurements (Drobinski et al., 1998; Higgins et al., 2013; Eder et al., 2015) etc. Spectral analysis of tower measured turbulence data can also give some insight into the nature of flux contributions from the lower frequencies (Y. Zhang et al., 2010; G. Zhang et al., 2014; Zhou et al., 2019; Gao et al., 2020).

Among these measurements, airborne EC measurements are one of the few that can directly measure the spatial distribution of 3D turbulence across a study domain (Mahrt, 1998, 2010). Moreover, with spatial transects, airborne measurements can directly sample contributions from larger (of the order of meso-β, meso-γ) scale persistent structures excited by surface heterogeneities. In contrast, for ground-based measurements these larger scale structures would have to drift by their field-of-view. Airborne transects through a study domain can also pass through multiple quasi-stationary eddies, giving robust statistics for the measured fluxes.

Here, we use airborne turbulence data collected over a heterogeneous mid-latitude forested landscape interspersed with creeks and lakes in the Chequamagon-Nicolet National forest near Park Falls, Wisconsin USA. Through this analysis we aim to address the following research questions:

1. Can spatially-resolved airborne eddy covariance identify spatial scales of surface-atmosphere fluxes over heterogeneous surfaces?
2. How do spatial scales of surface-atmospheric fluxes vary across the day and across seasons? What is the role of ABL stability and land surface variability in modulating these exchanges?
3. What are the ensuing implications for improving the surface energy balance closure or understanding scales of turbulent transport?

The airborne measurements were collected as part of the CHEESEHEAD19 field experiment (Butterworth et al., 2021), conducted from July to October 2019. The experimental study design aimed to sample the landscape transition from late summer to early fall and the associated ABL responses. The CHEESEHEAD19 airborne dataset presents a unique opportunity to analyse long periods of airborne EC over long legs (30 km) in a heterogeneous region over multiple times a year with differing patterns of surface sensible and latent heat fluxes. The dataset provides an extensive set of scenarios to investigate our research questions and derive principles from. To quantify and spatially localise contributions from all the relevant scales of transport we calculate the surface atmospheric fluxes through the wavelet cross-scalograms of the turbulent data (Strunin & Hiyama, 2004, 2005; Mauder, Desjardins, & MacPherson, 2007; Metzger et al., 2013). A wavelet based analysis can distinguish surface-atmosphere fluxes at multiple scales and quantify the contributions from larger scales, allowing us to resolve scale transport across space.

To those ends, we pose the following null and alternative hypotheses:

- H0: Mesoscale transport is an invariant, small fixed fraction of the total flux.
- HA: Persistent contributions of larger scale (in the range of meso-β to meso-γ) fluxes to the daytime sensible and latent heat fluxes exist with diurnal and seasonal variations.

2 Data and Methods

2.1 Experiment description

The Chequamegon Heterogeneous Ecosystem Energy-balance Study Enabled by a High-density Extensive Array of Detectors (CHEESEHEAD19) was a field campaign conducted from June to October 2019, in Chequamegon-Nicolet National Forest, Wisconsin, USA. The experiment was designed to intensively sample and scale land surface properties and the ABL responses to it across a heterogeneous mid-latitude forested landscape interspersed with creeks and lakes. Two main motivations for the field experiments were:

1. To determine how spatial heterogeneity of the surface impacts the local energy balance and atmospheric circulations
2. To evaluate how the presence or absence of these circulations influence the representativeness of single-point surface fluxes compared to the grid average

Measurements were made using a suite of observing platforms over a core 10x10 km domain (that would fit within a 'grid cell' of a weather/climate model) and a 30x30 km extended domain centred on the DOE Ameriflux regional tall tower[US PFa 45.9459 N, -90.2723 W]. EC fluxes have been measured nearly continuously at the US PFa tall tower since 1996 (Berger et al., 2001) and the study domain is well documented in previous studies that used flux data from the tall tower (Davis et al., 2003; Desai, 2014; Desai et al., 2015). The field campaign collected measurements of ground based and airborne fluxes, atmospheric profiles and surface environment at varying scales. Butterworth et al. (2021) gives a detailed overview of the field experiment design and all of the deployed instrumentation.

Figure 1 shows the land cover classes across the extended domain. The vegetation and land cover within the study domain is characteristic of a mid-latitude temperate forest, dominated by conifers, broadleaf deciduous trees and wetlands. The study domain is also interspersed with open water bodies, the largest being the Flambeau Lake to the North - Eastern sector of the domain. The presence of such a vertically and horizontally heterogeneous surface, with maximum canopy heights ranging from a couple of metres to 35 metres, gives a unique opportunity to study surface atmospheric exchanges over unstructured land surface heterogeneity where multiple surface properties and roughness elements vary at multiple scales, addressing a crucial gap in our current understanding (Bou-Zeid et al., 2020). Site descriptions of 17 flux tower sites, set up as part of the NCAR - Integrated Surface Flux Station (ISFS) network, within the core 10x10 km domain can be found at `http://cheesehead19.org`. This gives an idea about the variation in surface and vegetation properties across the domain. The extended 3 month duration of the field experiment also allows us to sample the shift in the surface energy budget partitioning as the study domain shifts from a latent heat - dominated, late summer landscape to a more sensible heat flux - dominated early autumn landscape.

2.2 Airborne intensive observations

Airborne turbulence data were collected over the extended domain with the University of Wyoming King Air (UWKA) research aircraft. The UWKA is a Beechcraft King Air 200T model, a part of the National Science Foundation's Lower Atmosphere Observation Facility that has been in use for insitu airborne measurements of cloud and boundary layer properties since 1977 (A. Rodi, 2011; Wang et al., 2012) Three seven-day Intensive Observation Periods (referred to as IOPs henceforth) were conducted during the experiment during each month from July to September when all the available field instrumentation were deployed simultaneously. During these IOPs the UWKA Research Aircraft flew linear transects across the domain on four days sampling turbulent measurements of wind velocities, temperature, water vapor, and CO2, at a frequency of 25 Hz [Table 1]. The airborne experiment was designed with the help of numerical experiments to maximise spatial coverage

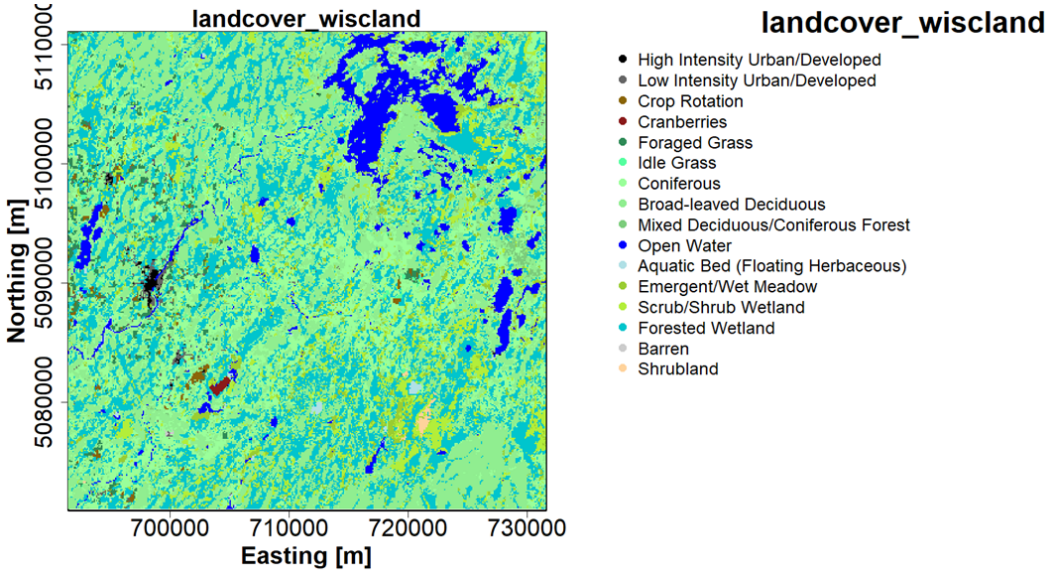

Figure 1: Land Cover classes for a 40x40 km area bounding the study domain from the Wiscland 2.0 landcover classification dataset

over the domain, ensure adequate sampling of larger scale eddies and ensure crew safety. Metzger et al. (2021) provides details about the numerical simulations, analysis framework and design strategy used to come up with the final flight patterns for the airborne measurements. Figure 2 shows these different patterns and their respective waypoints. Each research flight pattern was composed of flight transects connecting consecutive waypoints. We refer to these individual transects as flight legs. The flight legs were designed to be 30 km so that they extend about 10 km outside of the core 10x10 km domain to ensure that enough mesoscale contributions to the core 10x10 km domain could be sampled.

On each day there was a morning (1400 - 1700 UTC) flight and an afternoon (1900 -2200 UTC) research flight. Each research flight performed 30 km down-and-back transects at 100m and 400m above ground between two consecutive waypoints, alternating between straight and diagonal passes. The first leg of all transects was at 400m and the return legs at 100m. For example, from Table 1, on 2019 July 11th, the morning research flight was RF03 with the WE1 flight pattern. For RF03, from Figure 2, the first leg was from waypoint 1 to waypoint 2 at 400m and the second leg was back to 1 from 2 at 100m. Then the third leg would be from 1 to 4, diagonally at 400m and so on.

The primary scientific purpose of the higher 400m legs was to observe the temperature and moisture profiles using a downward pointing Compact Raman Lidar. The low-altitude legs were flown at 100m since this was the lowest altitude deemed safe to fly for the maximum forest canopy height of 35m. This also ensures that the measurements taken were in the surface layer and above the roughness sublayer of the forested domain. Wavelet cross scalograms of the atmospheric turbulence data from the 100m legs were used to calculate the surface atmospheric fluxes during the IOPs.

2.3 Wavelet Analysis

Wavelet analysis can be used to resolve the constituent scales of motion from spatial fluxes measured across flight transects and assess contributions from constituent scales (Mahrt et al., 1994; Strunin et al., 2004; Mauder, Oncley, et al., 2007). Wavelet transforms

Table 1: Dates, times, flight patterns of the flights analysed for all 3 IOPs

Date	UTC domain begin	UTC domain end	Flight Number	Flight Pattern	Wind Dir (deg)	Wind Speed (m/s)
2019-07-09	14:00	16:00	RF01	West-East 2	180	6
2019-07-09	19:00	21:00	RF02	West-East 2	210	5
2019-07-11	14:00	16:00	RF03	West-East 1	345	3
2019-07-11	19:00	21:00	RF04	West-East 1	45	5
2019-07-12	14:00	16:00	RF05	West-East 2	225	6
2019-07-12	18:00	21:00	RF06	West-East 2	225	5
2019-07-13	14:00	16:00	RF07	South East 2	330	3
2019-07-13	19:00	21:00	RF08	South West 1	330	3
2019-08-20	14:00	16:00	RF09	South East 1	215	3
2019-08-20	19:30	22:00	RF10	South East 1	180	1
2019-08-21	14:00	16:30	RF11	South West 1	0	5
2019-08-21	19:00	21:30	RF12	South West 1	315	6
2019-08-23	14:00	16:30	RF15	West-East 2	80	0.5
2019-08-23	19:30	21:30	RF16	West-East 2	120	3
2019-09-24	14:00	16:30	RF17	South East 1	230	4
2019-09-24	19:00	21:30	RF18	South East 1	180	5
2019-09-25	14:40	17:00	RF19	South West 1	270	5
2019-09-25	19:30	22:00	RF20	South West 1	310	5
2019-09-26	14:00	16:30	RF21	South East 1	270	3
2019-09-26	18:45	21:15	RF22	South East 1	265	5
2019-09-28	14:30	17:00	RF23	West-East 1	353	3
2019-09-28	19:00	21:30	RF24	West-East 1	15	3

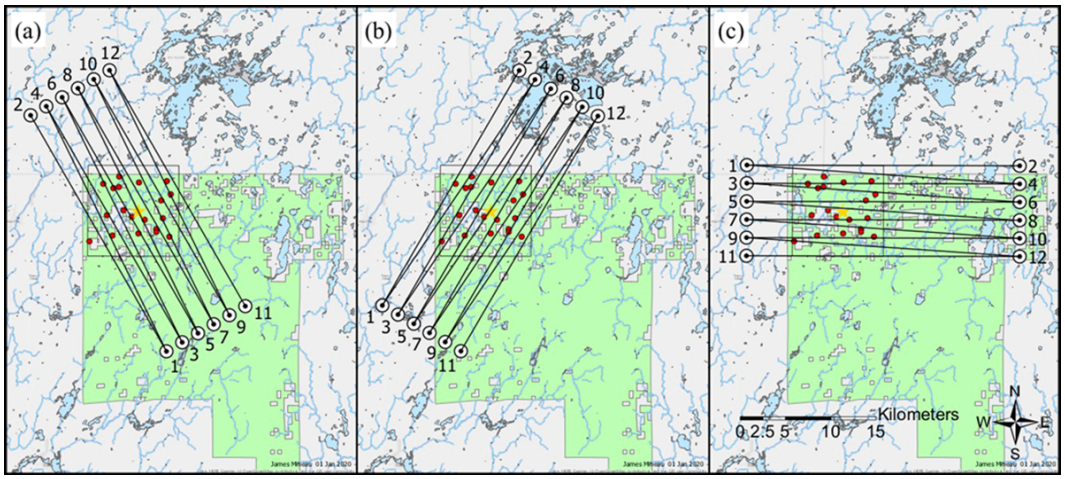

Figure 2: Three sets of waypoints define three distinct flight patterns, named after the starting location and direction of their first waypoint: (a) south-east (SE), (b) south-west (SW) , and (c) west-east (WE). Flying the numbered waypoints either in ascending order (SE1, SW1, WE1) or descending order (SE2, SW2, WE2) results in six distinct flight sequences that maximize data coverage under different wind conditions. Map credit: James Mineau, University of Wisconsin – Madison. [Metzger et al. (2021): Figure 14, published by Atmospheric Measurement Techniques, reproduced with permissions under https://creativecommons.org/licenses/by/4.0/]

involve convolving an input signal with a known, continuous wavelet function (Torrence & Compo, 1998) or a filter kernel, called as the mother wavelet. These mother wavelets are scaled and translated across the input data to extract the amplitudes and locations of matching details present in the input signal.

Airborne transects across a heterogeneous surface sample a patchy surface flux over the domain. Since both the scale and the location of the mother wavelet filter kernels can be adjusted, such an analysis can yield localised details matched to their scale (subject to the fundamental Heisenberg uncertainties). Because they can identify and localise varying frequency content they can be used for the analysis of in-homogeneous or non-stationary data (Cuxart et al., 2002; Strunin & Hiyama, 2004). So, a wavelet analysis of the CHEESEHEAD observations yields a space-scale mapping of the measured fluxes, throughout the day and across seasons.

For a signal $x(n)$ with a wavelet transform $W_x(a,b)$, the wavelet spectral energy can be defined as $W_x(a,b)^2$. Given two signals, $x(n)$ and $y(n)$, their co-variance can be estimated by integrating their co-spectral energy across the constituent scales as:

$$cov_{ab} = \frac{\delta j \delta t}{C_\delta N} \sum_{j=0}^{J} \sum_{n=0}^{N-1} \frac{W_x(a_j, b_n) W_y(a_j, b_n)^*}{a_j} \tag{1}$$

Where $*$ denotes a complex conjugate. We use the complex Morlet wavelet as the mother wavelet with $C_\delta = 0.776$ (Torrence & Compo, 1998). For the 25 HZ data, the time step, $\delta t = 0.04$ and δj, the discrete intervals in scale, is set as 0.125, setting up 8 octaves, following Torrence and Compo (1998).

A sample wavelet cross-scalogram and its associated scale-integrated flux space series is shown in Figure 3. Both the magnitude and phase of the contributions can be seen changing across scales through space in the cross-scalogram. Integrating subsets of the constituent scales can give the contribution from those ranges of scales to the total fluxes. This presents two impactful opportunities.

1. To quantify the contributions from specific spatial segments (research flight transects) of the sampled domain without neglecting contributions from higher scales
2. To quantify the contributions from different scales at specific spatial segments by integrating across subsets of scale (partitioning the measured fluxes into smaller and larger scales).

Following Mauder, Desjardins, and MacPherson (2007) and Strunin et al. (2004) we chose a cutoff wavelength of 2 km to distinguish between small-scale turbulent and larger mesoscale structures. The 2 km cutoff is a proxy for boundary layer height, which is assumed to be the highest scale for turbulent eddies. Mesoscale contributions were calculated as the difference between fluxes from all scales and the turbulent scale fluxes.

2.4 Flux measurement and data processing

The field experiment data was preprocessed by the UWKA research crew to include routine UWKA corrections and is hosted at the NCAR-EOL repository as part of the public CHEESEHEAD19 project data repository (French et al., 2021). Table 2 gives details of the UWKA instrumentation used for measuring aircraft and atmospheric state variables. The 25 Hz data was processed to pick out flight leg level data for each research flight, based on the leg timings from the flight way point catalogue. The data was processed using the eddy4R family of open source packages as described in Metzger et al. (2017). The production code is hosted in github following a DevOps framework for collaborative development. The workflows were adapted for the CHEESEHEAD data and the finalised repository structure

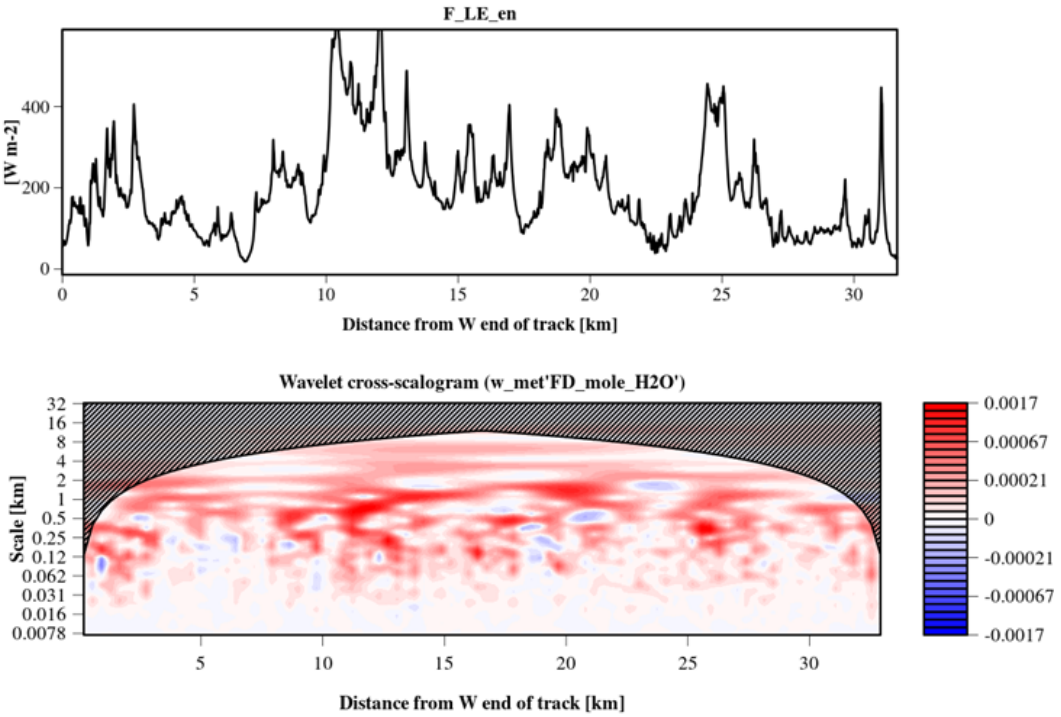

Figure 3: A sample wavelet cross-scalogram and its associated flux space series. At the bottom is a wavelet cross-scalogram between vertical velocity and water vapour mole fraction illustrating the scale-resolved spatial contributions along one flight leg. At the top is the scale integrated version of the same in energy units, giving the latent heat flux space series. The red shaded amplitudes denote positive contributions, while blue shades denote negative and white neutral. Hashed out portions represent the cone of influence for edge effects.

Table 2: Univerity of Wyoming King Air instrumentation details

Measurement	Instrument	Description
	Aircraft State	
3D position, ground velocity, orientation, Body-axis longitudinal/lateral/vertical acceleration	Applanix AV 410 GPS/Inertial Measurement Unit	Applanix Position Orientation System for Airborne Vehicles; combined solid-state/GPS system with real-time differential corrections; higher accuracy post processed data available (Haimov & Rodi, 2013)
Altitude	Stewart Warner APN159 radar altimeter	Altitude above ground level Range:0 - 60000 ft(18288 m); accuracy 1%; resolution: 0.24 ft (0.07 m)
Airspeed	Honeywell Laseref SM Inertial Reference System (IRS)	Range:0-4095 kts; accuracy: 13.5 ft/s ; resoluton: 0.0039 kts
flow angles	Rosemount 858AJ five-hole gust probe	Range:+-15; accuracy:0.2; resolution:0.00015
	Atmospheric State	
Air temperature	Reverse-flow housing with Minco platinum-resistive element (A. R. Rodi & Spyers-Duran, 1972)	Range: -50 to +50 C; accuracy: 0.5 C ; resolution: 0.006 °C
Wind Components	Applanix AV 410 GPS/Inertial Measurement Unit	Earth relative 3D wind
Atmospheric Pressure	Rosemount 1501 HADS	High Accuracy Digital Sensing module static pressure, corrected for dynamic effects (A. R. Rodi & Leon, 2012) ; Range: 0-1034 mb; accuracy : 0.5 mb, resolution: 0.006 mb
Water vapor	LICOR Li-7500A	LI-COR LI-7500 open-path CO2/H2O Gas Analyzer

is maintained as Docker images to preserve the same dependencies and result reproducibility across platforms.

A spatial series of wavelet covariance fluxes is calculated from the wavelet cross-scalograms for 1000m moving windows (Metzger et al., 2013). Random flux sampling errors are calculated for the moving windows following Lenschow et al. (1994), Lenschow and Stankov (1986). Adaptive high frequency corrections were applied to the turbulence data following (Nordbo & Katul, 2013). Further, while creating summary statistics and figures an absolute threshold of 10 Wm^2 was applied for sensible and latent heat fluxes to ensure that the fluxes are well resolved. A hard threshold of (-400, 1000) Wm^2 was set for the LE space series and (-50,400) for the H series to remove spurious measurements.

2.5 Scale-resolved fluxes vs land surface

To investigate how the measured mesoscale contributions vary over the course of a research flight and spatially over the domain, the measured fluxes are back–projected to their surface source as gridded two-dimensional data following the flux topography method of Mauder, Desjardins, and MacPherson (2008). Flux topographies are the footprint-weighted flux contributions measured across the domain from the airborne data (Amiro, 1998). To get information about the land surface we are using the Wisclan 2.0 land surface information for land surface classes for a 40x40 km domain at 100m resolution. The flux topographies are also calculated over the same grid.

The calculated fluxes are then projected back to the surface grid, weighted at each grid cell by the flux footprint. Footprint of a flux measurement refers to the effective finite measurement area upwind of the sensors from where the eddies are being sampled from (Foken et al., 2006). Kljun et al. (2004) is a parameterisation of a Lagrangian model (Kljun et al., 2002). Since this is not crosswind-integrated, Metzger et al. (2013) combined it with a Gaussian crosswind dispersion function. This is implemented in the analysis currently.

A flux topography was calculated like this for each flight leg of a research flight and then the cumulative footprint weighted contribution F_{ij} is calculated at each grid cell for a research flight (Kohnert et al., 2017).

$$F_{ij} = \frac{\sum_j^N (\sum_i^M f_{i,j} * g_{i,j})}{\sum_j^N (\sum_i^M g_{i,j})} \tag{2}$$

The study domain is sampled as the UWKA passes by adjacent surface locations and their contributions to surface-atmospheric fluxes are weighted by flux footprint, thus giving a space-scale resolved snapshot of surface-atmospheric exchanges over the course of the research flight. Source areas with really low footprint values ($< 0.05\%$) are excluded from the analysis.

3 Results

To have a sense for the variation and evolution of measured turbulent and meso- scale fluxes we start by looking at how they vary seasonally across the IOPs in Section 3.1. We present the seasonally averaged and scale-resolved contributions. Following this, we present the domain-averaged and scale-separated diel data of the fluxes for each of the IOPs. Then the flight averages for all of the research flights analysed here are also presented. In Section 3.2 we discuss the observed relationship between mesoscale transport and local ABL stability. Then, we investigate the composition of land cover contributions within the footprint of flight legs and how those might relate to the observed mesoscale transport in Section 3.3.

3.1 Seasonal and diurnal variations

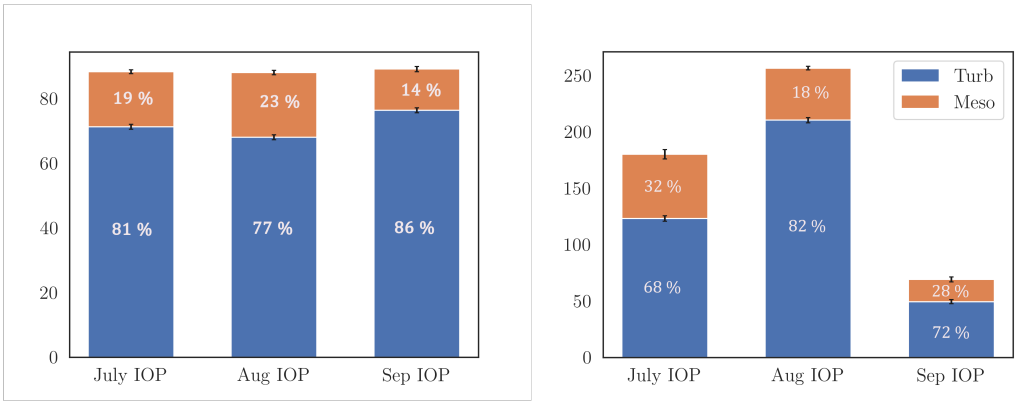

(a) Sensible heat flux $[Wm^2]$ at 100m

(b) Latent heat flux $[Wm^2]$ at 100m

Figure 4: Mean turbulent(blue) and mesoscale (orange) (a)H and (b)LE fluxes for the three IOPs showing seasonal flux transitions. The flux percentages of the total are shown in white within the bars.

IOP averaged flux magnitudes reflect the seasonal shift in the landscape (Figure 4). IOPs were conducted from late summer in the start of July to early autumn at the end of September 2019. In July the study domain is latent heat flux-dominated and towards the end of September as senescence starts to set in, it transitions to a sensible heat flux-dominated landscape. The mean sensible heat flux magnitude for all scales does not change substantially between the three IOPs and remains around 89 Wm^2. However, there is a

substantial variation in the magnitudes of the latent heat fluxes measured across the months. The measured total LE is higher than the total H in the July and August IOPs, increasing from 179 ± 5 Wm^2 to 256 ± 3 Wm^2 and then reduces to 69 ± 3 Wm^2 in the September IOP (Figure 4 and Table S1) , falling below the total sensible heat flux measured [89 ± 1 Wm^2]. The percentage mesoscale and turbulent contributions to the total measured fluxes also show a seasonal variation for the sensible and latent heat fluxes. For the sensible heat flux, the percentage turbulent contribution for the July IOP is 81%, which reduces to a further 77% in August and then increases to 86% in September. Similarly, for latent heat fluxes, the percentage turbulent contribution for the July IOP is the least, at 68%, increasing to 82% in August and then decreasing to 72% for September. When a particular heat flux dominated the surface atmospheric exchange it also had the lowest percentage mesoscale contribution among the IOPs. In August when the total(turbulent + mesoscale) latent heat flux magnitude is at its maximum at 256 ± 3 Wm^2, the mesoscale fraction of the same is at its minimum, at 18%. Similarly, when the evaporative fraction is at its minimum September at 0.76, the sensible heat mesoscale fraction is also at a minimum at 14%. The sensible heat flux data averaged across the domain and all flight days shows a diurnal cycle for all of the IOPs (Figure 5 column 1, black lines). The calculated turbulent scale fluxes follow the same patterns closely, but mesoscale fluxes do not. For the July IOP data, the total sensible heat flux peaks at 128.8 ± 1.31 $Wm2$ around 11:20 CDT. In August the sensible heat flux maximum is of the same order, at 121.1 ± 1.3 Wm^2 but shifted to later in the afternoon around 15:20 CDT (Figure 5c). The measured fluxes in the August IOP also show sustained values of the order of 100 Wm^2 from late morning to after noon (10:50 - 15:30 CDT) until later in the day towards the end of the afternoon.The September IOP sensible heat flux data has a more pronounced peak at 148.7 ± 1.5 Wm^2. Our scale analysis reveals that this clear diurnal signal is present only for the turbulent scale fluxes which follow the total fluxes diel pattern closely for most of the flight day. In the July IOP the calculated mesoscale sensible heat fluxes peak around 30.8 ± 0.8 Wm^2 before noon and in the afternoon there are sustained values around 20 Wm^2 till later in the evening towards the end of the research flights. This can also be seen reflected in the difference between the total and turbulent flux diel plots in Figure 5 a. Similarly for the August IOP, mesoscale fluxes show sustained values in the afternoon around 25 Wm^2, peaking at 34.8 ± 1 Wm^2. Sensible heat mesoscale values are the lowest in the September IOP as observed earlier in the IOP averaged data. The median value for the IOP data is 11 Wm^2, and the maximum value observed was 18 ± 0.7 Wm^2 around 14:30 CDT.
The latent heat fluxes do not show such a clear diurnal variation for the domain averaged data. The domain averaged flux magnitudes are of the same order of magnitudes as the IOP averaged values presented earlier.

The total fluxes measured for all research flights analysed is presented in Figure 6. This picture at a research flight level reflects the seasonal variation detailed in Figure 4. Flux measurements from Research Flights 2 (July 9th afternoon) and 3 (July 11th morning) stand out in the July IOP data (July 09 - 13) with total fluxes measured at 430.2 Wm^2 and 436.5 Wm^2. This is due to increased contributions from turbulent latent heat fluxes for the two flights (Figure S2). The mesoscale contributions measured were of the same order of magnitude as other days of the IOP. Similarly, Research Flight 23 (Sep. 28th morning) stands out in the September IOP (Sep. 24 - 28) with measured turbulent fluxes the same order of magnitude as the late summer IOPs. This was due to an increase in the measured turbulent latent heat fluxes (Figure S6) due to a rain event earlier that day.

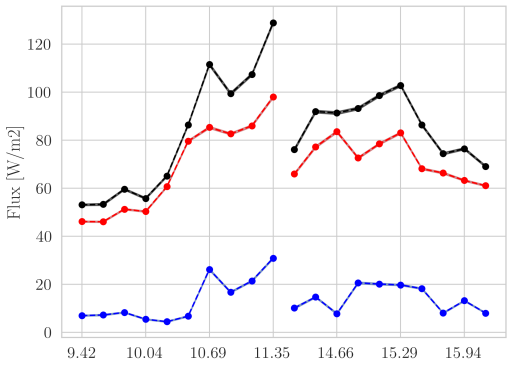

(a) Leg averaged, diel sensible heat fluxes for July IOP

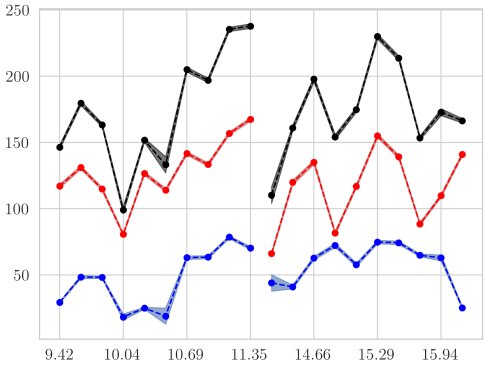

(b) Leg averaged, diel latent heat fluxes for July IOP

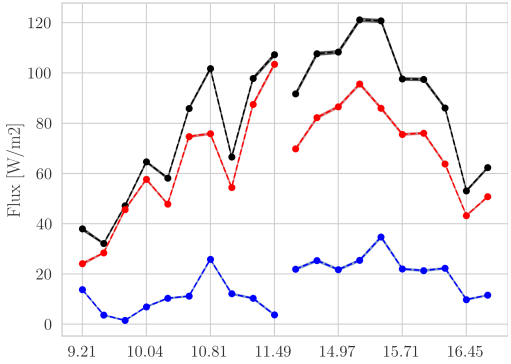

(c) Leg averaged, diel sensible heat fluxes for August IOP

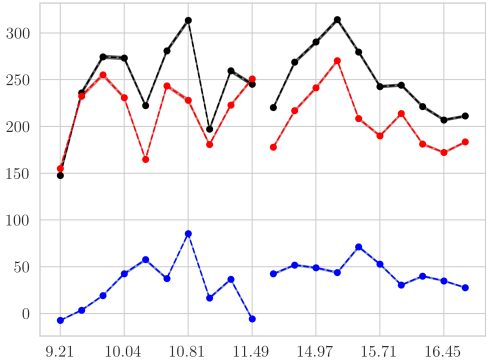

(d) Leg averaged, diel latent heat fluxes for August IOP

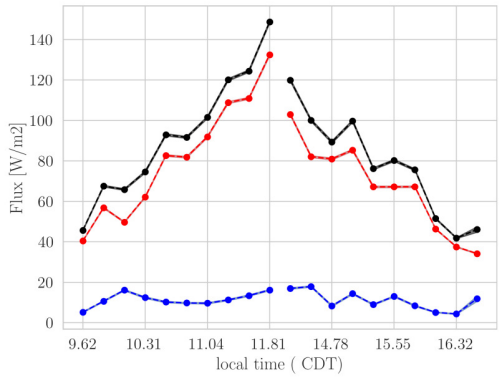

(e) Leg averaged, diel sensible heat fluxes for September IOP

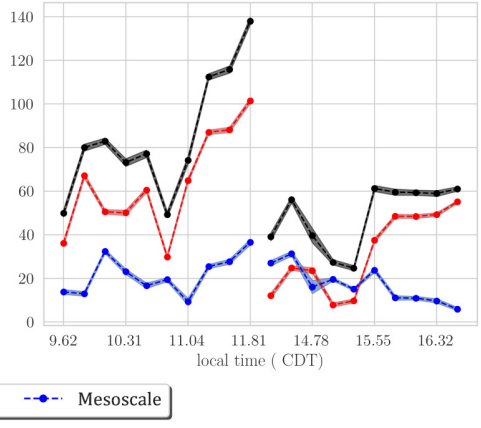

(f) Leg averaged, diel latent heat fluxes for September IOP

Figure 5: H and LE fluxes averaged for flight legs at the same time across all analysed days for the three IOPs. Every day had 2 research flights, a morning and afternoon flight. Every flight had 20 flight legs, numbered 1 to 20. Each data point is the mean value of fluxes measured from all flight legs at the same time of day in an IOP. The scale-resolved diel time series is shown. x axis shows the mean local time of those flight legs. Since the x axis is ordered according to the flight leg timings, the 2.5 hours break between the end of the morning leg and the start of the afternoon leg is included as discontinuities in the plots. Each row shows data for an IOP. The first column shows the sensible heat flux values and the second column shows the latent heat flux values

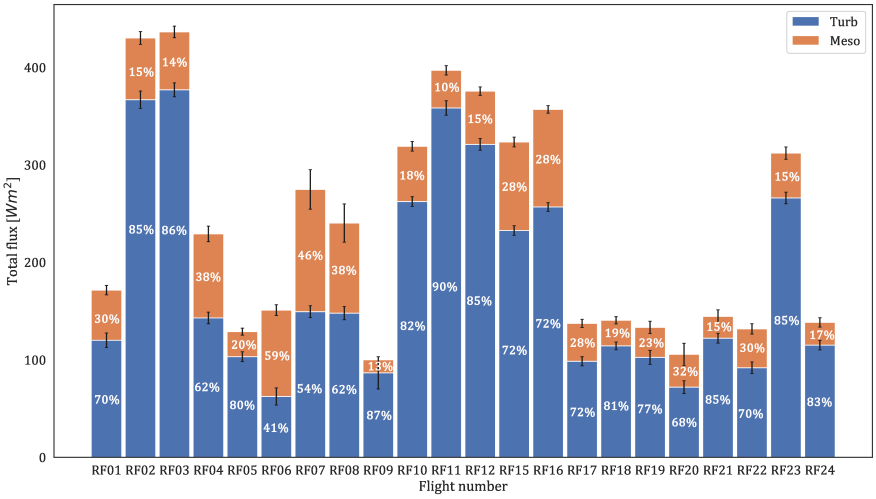

Figure 6: Total (H + LE) fluxes measured on each research flight for all the processed research flight data. Each bar graph represents the mean, scale-resolved flux for a research flight. The x axis shows the research flights and y axis flux magnitudes. Turbulent fluxes in blue and mesoscale fluxes in orange. Percentage contributions in white numbers.

3.2 ABL and land surface drivers of transport

ABL dynamics

The turbulent surface layer scaling parameter $\zeta = \frac{z}{L}$, where z is the measurement height and L the Obukhov length, can be regarded as a stability parameter (Stull, 1988). Negative values of ζ close to 0 indicate a statically neutral surface layer and as the value decrease as the surface layer becomes more statically unstable.
Histograms of median ζ values from flight legs show that the August IOP is more convective than the other two IOPs with more data points within the $\zeta <$ -1 range (Figure 7). On the other hand the September IOP looks strongly shear driven, with most of the data falling within $\zeta \in$ [-1 , 0). In this regard, July and September IOPs seem to be dynamically similar.

To understand how scale-resolved contributions vary with ABL dynamics, we looked at the PDFs of sensible heat mesoscale fractions for shear driven ($\zeta \in (-1, 1]$) vs convectively driven ($\zeta \in (-20, 1]$) ABL (Figure 8). The two distributions were found to have significantly different locations for all 3 IOPs using the Mann-Whitney U rank test with 95% confidence. This indicates that there is a statistically significant higher fraction of mesoscale transport observed in convectively driven ABL across all the three IOPs.

For latent heat fluxes, the kernel density estimates of mesoscale fractions for the July and August IOPs show higher mesoscale fluxes for convective cases (Figure 9). Performing a Mann-Whitney U rank test again showed that the distributions have significantly different values for the two stability regimes at 95% confidence. However, for September IOP the mesoscale transport does not have a preference between a shear or convectively driven ABL. Even though July and September IOPs have similar ABL stability distributions their latent heat mesoscale transport does not show the same behaviour, hinting at the role of seasonality through changing surface characteristics and insolation.

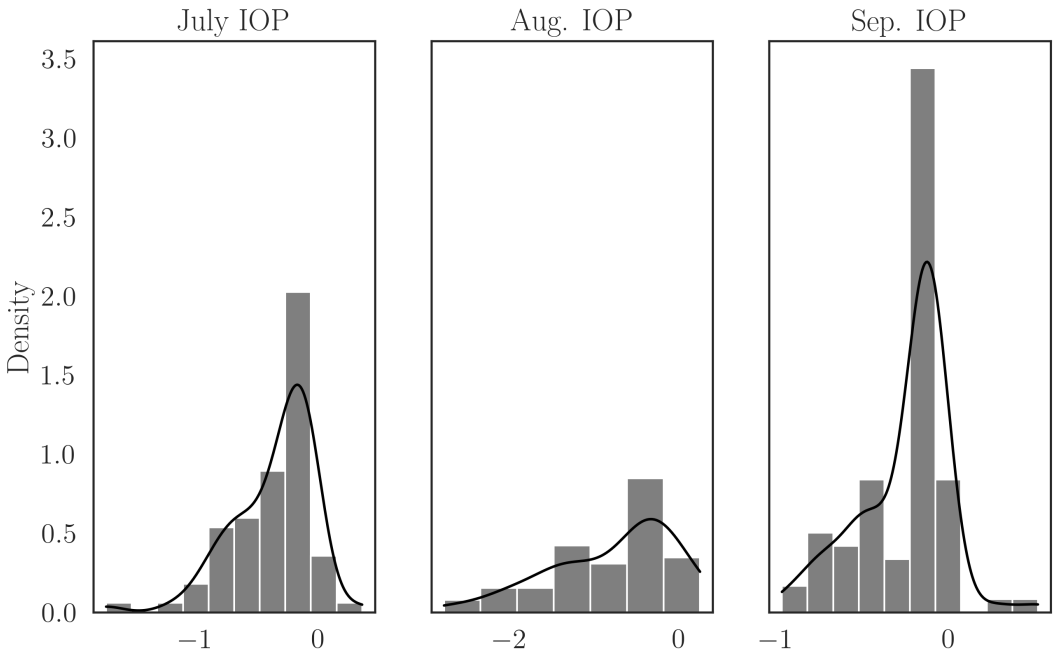

Figure 7: Histograms of median ζ values for flight legs for all three IOPs

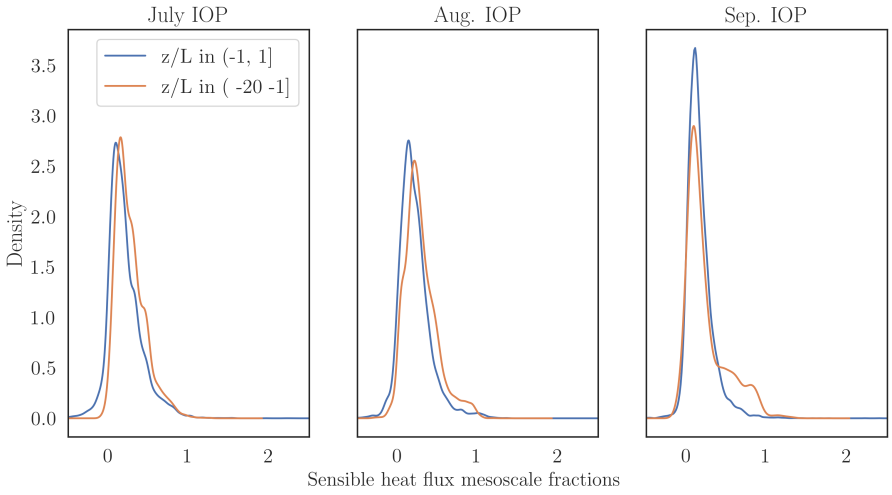

Figure 8: Kernal density estimates of sensible heat flux mesoscale fractions for all three IOPs

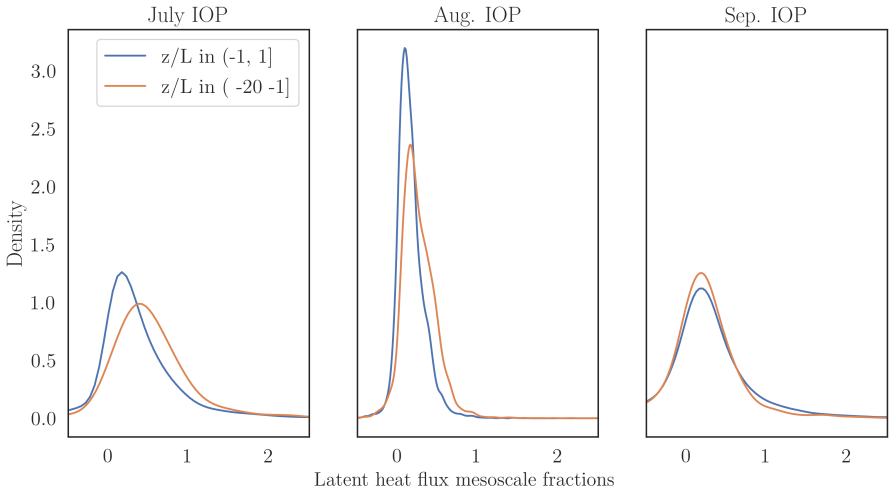

Figure 9: KDE plots of latent heat mesoscale fractions for all three IOPs

The KDE plots for sensible and latent heat mesoscale fractions show values > 1 and < 0. These occur when the measured mesoscale and turbulent fluxes are out of phase with each other. For both sensible and latent heat fluxes, the histograms of turbulent and mesoscale fluxes when the mesoscale fraction is greater than 1 shows higher, positive values of mesoscale fluxes and lower negative values of turbulent scale fluxes (Figure S8). Indicating that the mesoscale fluxes dominate such instances, driving the fraction to be over 1. Similarly for mesoscale fractions < 0, the sensible heat flux histograms for scale-resolved fluxes show higher, positive values for turbulent fluxes and lower negative values for mesoscale fluxes causing the mesoscale fraction of the total flux to be negative (Figure S7). The same phase difference between turbulent and mesoscale fluxes can be seen in the latent heat fluxes too, although they behave more uniformly.

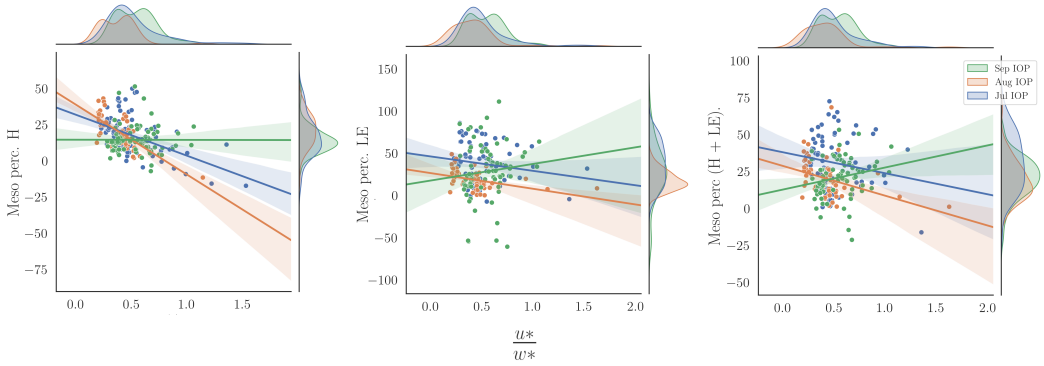

Figure 10: Scatter plots of mesoscale flux percentages vs u*/w* for all three IOPs. Flight leg level averaged values are presented. Outlier removal was done for the mesoscale percentage values based on median absolute deviation (Boris Iglewicz and David Hoaglin 1993). Linear regression lines with 95% confidence limits are also included for the same. Kernel Density Estimate plots for each distributions are drawn on their respective axes.

u*/w* is a non-dimensional parameter that can succinctly capture the competing effects of free and forced convection in the ABL. If the ABL is strongly shear driven, one would expect higher u* values and lower w* values, leading to higher values for u*/w* and vice versa for a convectively driven ABL. Kernel density estimates of u*/w* and the scatter of percentage mesoscale fluxes vs u*/w* reflect the ζ distribution characteristics for the 3 IOPs seen earlier in Figure 7. September IOP has a median u*/w* value of 0.55, higher than the July (0.45) and August (0.43) IOPs, indicating more shear driven surface atmospheric transport. Similarly, the distributions for July and August IOPs are also similar with the august IOP having a slightly lower median value indicating more convectively driven transport.

The meso H percentages show a decreasing trend with increasing u*/w* values in July and August IOPs indicating higher mesoscale transport during more convective scenarios. This is especially clear in the almost flat regression line for the September IOP scatter. However, LE mes-scale flux percentages behave differently. For the September IOP they show and increasing trend with increasing values of u*/w*. Figure 4b also shows high (29%) mesoscale fluxes for LE in the September IOP. This once again illustrates that there is substantial mesoscale latent heat fluxes in both shear and convectively driven ABLs. The scatter of total (H+ LE) mesoscale flux percentages gives a combined picture of the H and LE characteristics as seen from the first two plots in Figure 10. Here we see increasing mesoscale flux percentages for each IOP according to the dominant ABL stability, with increased contributions for convective cases in the July and August IOPs and for shear driven cases in the September IOP.

Distribution of land cover classes

Most of the footprint contributions in the study domain comes from wetlands, coniferous and broad leaf deciduous forests, with wetlands dominating the source areas (Figure 11). Further breaking down the wetland class, we find that most of the contributions come from the forested wetlands in the domain.

Flux contributions by land cover:

For a more detailed investigation of changes in footprint contributions with time, flight leg level footprint contributions were also calculated. This gave fractional footprint contributions for each flight leg from all the land cover classes. Using this data, the land cover class with the maximum fractional footprint contribution for each flight leg was picked. The same overall pattern across the IOPs seen in Figure 4 is repeated in Figure 12 as well, with regards to the magnitudes of the fluxes across IOPs and the scale-resolved percentages. The broadleaf deciduous forests have the lowest percentage turbulent fluxes in the July IOP, with only 37% for LE and 70% of H.
The kernel density estimates for mesoscale fractions did not show significant differences between the three major land cover classes.

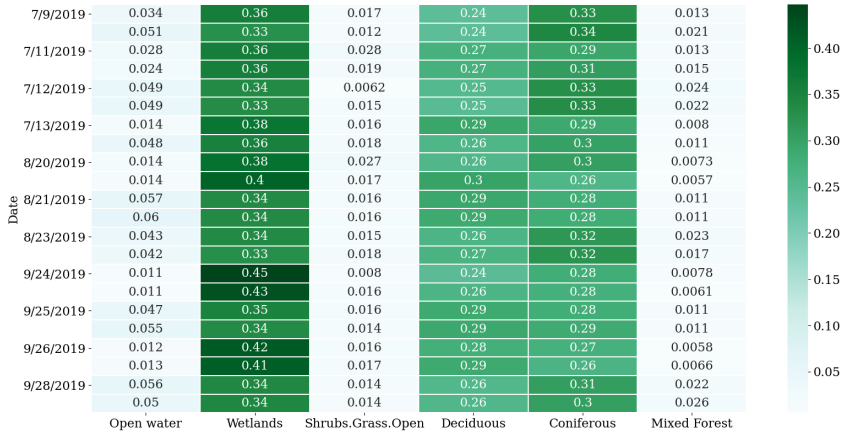

Figure 11: Fractional footprint contributions for the major land cover classes within the study domain for each research flight. Land cover class data from wiscland 2.0 database as shown in fig. 1 for the 40x40 km domain. Land cover classes have been grouped into open water, wetlands, deciduous forests, shrubs/grass/open land, coniferous and mixed forests. The X axis shows the land cover class, and the Y axis rows are the airborne campaign dates. The numbers inside the boxes show fractional footprint contributions and they are also highlighted according to the color bar

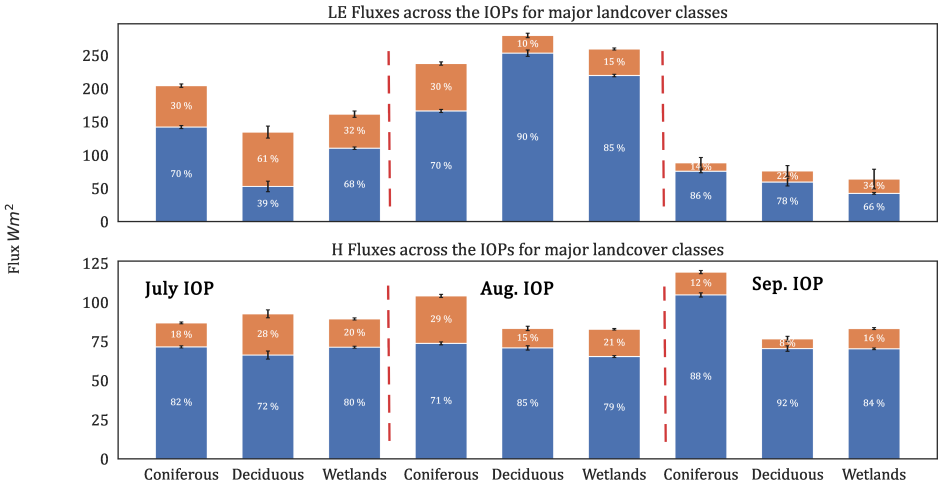

Figure 12: Turbulent and mesoscale sensible and latent heat fluxes measured for the major land cover classes across the IOPs. For all research flights analysed, the land cover class with the maximum footprint contribution to the measured fluxes per flight leg was picked. Then this was grouped by their respective IOP. Turbulent fluxes in blue and mesoscale fluxes in orange. Panel a on top shows the LE fluxes and panel b at the bottom shows the H fluxes. Bar graphs for each of the three IOPs are separated by vertical dashed red lines and ordered as contributions from coniferous, deciduous forests and wetlands within each IOP group

3.3 Space scale resolved fluxes

We present a case study for one good flight, with a sample flux topography for a summertime morning flight, RF03, conducted on July 11th, 2019 from 09:20 to 11:30 CDT. The flight did east -west transects across the domain, starting from the northern edge and moving to the south. Aircraft logs for the day mention observing shallow cumulus clouds indicating local convection and weak winds for this day. This ensured that the flight transects had a good footprint coverage over the domain for this research flight.

Spatially resolved sensible and latent heat flux topography maps (Figure 13a) show similar order of magnitude values as the IOP averaged behaviour in Figure 4. The latent heat flux dominates and shows more spatial variability than the sensible heat flux. Spatial distribution patterns of both the fluxes do not look similar either. The percentage mesoscale contributions for the two fluxes also show differing spatial patterns (Figure 13b). These flux topographies illustrate the fact that the CHEESEHEAD tower sites inside the study domain sample differing Bowen ratios within the same 10x10 km domain and there are spatially varying , concomitant mesoscale surface-atmospheric transport. This would imply that not all of the towers are sampling the same flux transport and the mesoscale transport associated with their locations would also be different. The flux topographies indicate stronger mesoscale contributions towards the southern edge of the domain in the sensible heat flux plots (Figure 13b). This is due to the inherent time dependency in calculating the topographies from the flight transects. Each research flight duration is about 2 hours. This particular flight started measurements at the north end of the domain in early morning and by the time it reached the southern edge it was close to noon and by then a fully developed CBL would have formed. Sensible heat mesoscale fluxes develop more later in the day as well (Figure 5a, 5c). The scale-resolved fluxes for latent heat for this flight indicate that the turbulent and meso peaks do not align in space (Figure 13c). Flux topographies for research flights in the August and September IOPs are presented in the supplement along with the standard error percentages for the footprint weighted fluxes (Gatz & Smith, 1995) following Kohnert et al. (2017).

The inherent time dependency of the topographies leads to source strength non-stationarity, since the surface heat flux magnitudes change over the course of the measurement.This makes the flux topographies harder to interpret. A fusion LST product over the domain (Desai et al., 2021) for the measurement time shows a high amplitude west-east band in the centre (Figure 13d). mesoscale gradients can be observed close to this band in the latent heat flux plots of Figures 13.b and 13.c. However, since the large scale transport would be from quasi stationary structures we can't directly link the same to land cover or LST gradients in our current analysis framework.

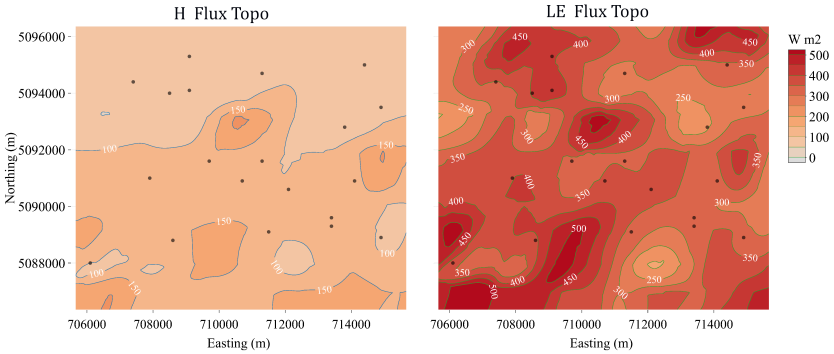

(a) Sensible and latent heat flux topographies

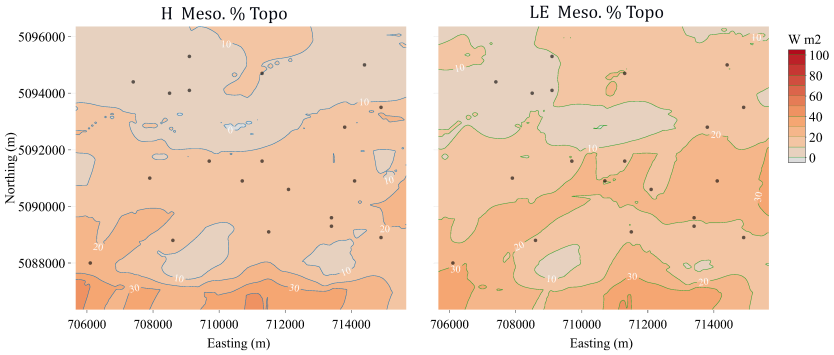

(b) Percentage mesoscale contribution in the flux topographies

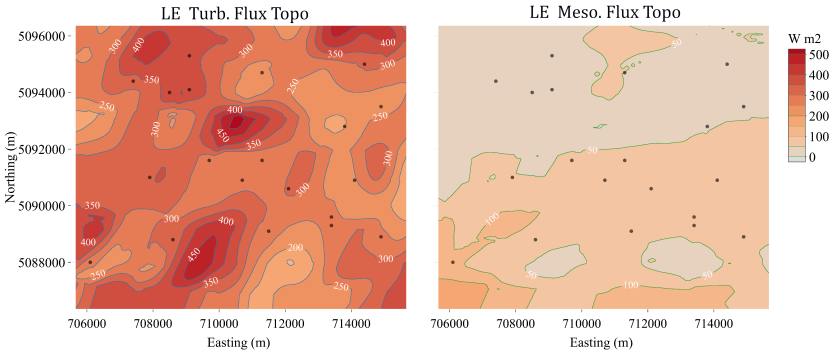

(c) Turbulent and mesoscale contributions of the latent heat flux topographies

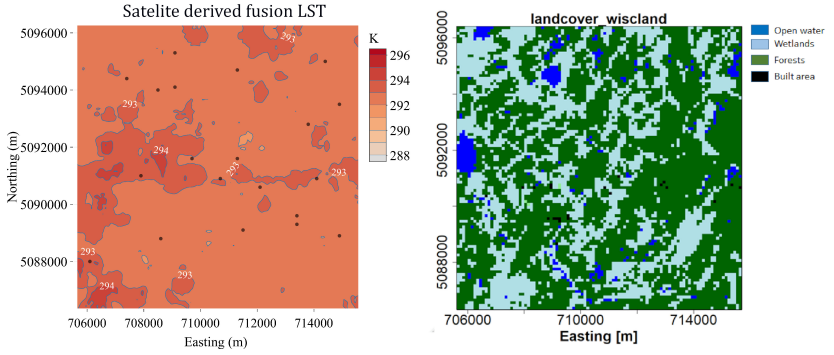

(d) Surface properties, LST (left, (Desai et al., 2021)) and land surface classes (Wiscland 2.0)

Figure 13: Flux topographies for Research Flight 03 in the July IOP, 11 Jul. 09:20 to 11:20 CDT over the 10x10 km CHEESEHEAD core domain. The brown dots are the NCAR-ISFS tower locations. (a) Sensible (left) and latent (right) heat flux topographies,(b) percentage mesoscale contributions to the sensible (left) and latent(right) heat flux topographies, (c) scale-resolved, turbulent (left) and mesoscale (right) topographies for the latent heat flux and (d) distribution of land surface properties across the domain.

4 Discussion

Implications for Surface - Atmospheric Transport and Surface Energy Budget closure

We observed higher fractions of mesoscale transport for sensible and latent heat fluxes in convectively driven ABLs as shown in the KDE plots (Figure 8 and Figure 9) in section 3.2. Previous observational studies have noted the inverse relationship between tower measured surface energy balance imbalance and u* (Stoy et al., 2013; Eder et al., 2015), indicating that strong mechanical mixing in shear driven ABL leads to larger turbulent transport. Our findings also indicate the same, that lower frequency transport seems to have a preference for convectively driven boundary layers. The dependency of latent heat fluxes is more complicated than the sensible heat flux transport.

Using data from the LITFASS 2003 field experiment in Germany Foken (2008) Foken et al. (2010) showed that area averaged surface flux measurements reduce the surface energy budget residuals. This, combined with the observations that the residuals are worse for sites with more heterogeneous surfaces, leads to his hypothesis that what has remained unaccounted for in the budgets could be the transport due to quasi-stationary secondary circulations tied to landscape heterogeneity. The synthesis study by Stoy et al. (2013) found consistent energy balance non closures across the sites and more importantly, noted that non-closure is linked to the degree of landscape heterogeneity, quantified using MODIS products and GLOBEstat elevation data. Since then a growing body of research has suggested that quasi-stationary low-frequency eddies in the ABL tied to land surface heterogeneity can play an important role in surface-atmospheric transport.

LES studies with homogeneous (S. T. Salesky et al., 2017; Li & Bou-Zeid, 2011) and heterogeneous (Margairaz et al. (2020), idealised heterogeneities) surface forcings have observed secondary circulations in the ABL transition from convective rolls to a cellular structure as the ABL becomes more convectively unstable. Margairaz et al. (2020) notes that for their simulations, with imposed surface temperature heterogeneities in irregular rectangular patches, the convective-cell structure adjusts to the imposed surface temperature variations. The surface atmospheric transport associated with these circulations would be missed by tower based measurements unless they are either swept across the spatially-stationary measuring points by the mean wind or only if the point measurements happen to be in their vicinity (Mahrt, 2010; Charuchittipan et al., 2014). These studies along with observations of better closure with longer averaging times and spatial measurements have led to a leading hypothesis that the surface energy balance closure problem is in fact a problem of scale (Foken, 2008; Foken et al., 2010; Mauder et al., 2020)

Large scale organisations in the form of longitudinal roll vortices, aligned with the mean wind can be generated in daytime convective boundary layers (Etling & Brown, 1993) while stationary circulations can also be induced by horizontal variations in surface roughness and heat flux (Desjardins et al., 1997; Sun et al., 1998). LES studies have shown that over homogeneous surfaces, strongly unstable conditions can lead to the formation of standing convective cells akin to those that form in Rayleigh-Benard convection (Kanda et al., 2004; De Roo & Mauder, 2018). Over heterogeneous surfaces these free convective cells tend to become quasi-stationary secondary circulations, tied to the surface temperature, roughness or vegetation gradients (Inagaki et al., 2006; Maronga & Raasch, 2013). Such secondary circulation cells can lead to a persistent local-mean advective transport, leading to an underestimation of surface energy exchange (Morrison et al., 2021)

(Desai et al., 2021) presents a 50 m resolution fusion LST product for the same study domain, derived using a fusion of land surface model and satellite products. They note that the spatial standard deviation of the fusion product increases towards autumn and is also high for summer afternoons, with higher LST spatial gradients. This could be playing a role

in the higher sensible heat mesoscale fluxes observed in the late morning and afternoon for the July and August IOPs (Figures 5a and 5c)

In this regard, using wavelet methods on high-frequency airborne data has allowed us to retain the larger scale surface-atmosphere transport across the heterogeneous study domain and account for relevant transport scales. The mesoscale contributions are not a fixed fraction of the total or turbulent fluxes but vary throughout the day and as the landscape undergoes seasonal transitions (Figure 4 and Figure 5). The scale-resolved sensible and latent heat fluxes do not behave similarly either. During the August IOP, (08/20 to 08/23), the measured Bowen ratio is the lowest at 0.3 and this IOP has the lowest meso fraction for latent heat fluxes. Similarly, during the September IOP in early autumn (09/24 to 09/28) , the Bowen ratio is the highest at 1.3 and mesoscale sensible heat flux fraction was the lowest during this IOP. The total mesoscale flux percentages for July IOP = 29%, August IOP = 20% and September IOP = 21%. The total percentages are closer in magnitude because of the seasonal sensible and latent heat flux balance. It is interesting to note that the August and September IOPs with very different Bowen ratios have the same mesoscale flux percentages.

The observed spatial variations of the mesoscale transport, would not be sampled by stationary tower measurements within the domain (Figure 13, Figures S9, S11, S12, S15, S16). The flux topographies calculated present a direct and physics-based flux map over the domain for the research flights analysed, providing a scale-resolved spatial distribution of sensible and latent heat fluxes. They show persistent areas of large scale flux contributions within the study domain which could be linked to variations of land surface properties. However, they are inherently limited by the foot prints of airborne transects and can only be extrapolated within those flight transect footprints. Moreover, the experimental design introduces a temporal element to the topographies. Even though spatially adjacent flight transects during a single flight are only about 6-8 minutes apart , a research flight across the domain takes about 2.5 hours. Since they don't represent a single snapshot in time, attributing sources for the fluxes and linking flux gradients and surface gradients can be complicated. This would require a space-time aligned dataset from high resolution numerical simulations like LES or products from scale aware scaling algorithms such as ERFs (Metzger et al., 2013).

5 Conclusions

We present a systematic regional-scale observational analysis over a heterogeneous domain that quantifies the multi-scale nature of sub-grid scaling and patterning. The CHEESEHEAD19 field experiment provided a unique dataset to diagnose and quantify the diel and seasonal contributions from large scale transport over the study domain as its surface energy balance shifts from a more latent heat flux-dominated late summer landscape to a more sensible heat flux-dominated early autumn landscape.

Using airborne measurements from this comprehensive field experiment dataset we sought to answer whether spatially resolved airborne eddy covariance can identify spatial scales of surface-atmosphere fluxes over heterogeneous surfaces? Applying wavelet analysis to the airborne flux measurements from the field experiment data allowed us to evaluate and spatially resolve the mesoscale contributions at 100 metres above ground over the heterogeneous landscape. We looked at the diel and seasonal variability of the scale-resolved fluxes. The measured latent heat flux magnitudes had more pronounced seasonal changes than the sensible heat fluxes. Meanwhile, the measured domain-averaged sensible heat flux values had a more pronounced diurnal cycle. We observed larger mesoscale transport for sensible heat fluxes in convectively driven ABLs across the three IOP scenarios, while for latent heat fluxes only the July and August IOPs showed more fractional mesoscale transport in convectively driven ABLs. For the September IOP, which had mostly shear driven ABL cases, we did not find any significant change between the fractional mesoscale transport in

convectively and shear driven ABLs. We hypothesise that the larger scale transport measured in our study could be linked to organized structures in the ABL as has been reported in previous numerical (Kanda et al., 2004; Inagaki et al., 2006; S. Salesky & Anderson, 2020; Margairaz et al., 2020) and observational (Eder et al., 2015; Morrison et al., 2021) studies. The flux topography case studies indicate that the mesoscale transport spatial variability would be missed by tower measurements in the domain. Areas of persistent contributions in the domain could be linked to the presence of co-located forested wetlands, creating roughness and thermal surface heterogeneities.

From our observations and analyses we reject our null hypothesis that the mesoscale transport is an invariant, small fixed fraction of total flux. We conclude that our alternate hypothesis, persistent contributions of larger scale (meso-β to meso-γ) fluxes to the daytime sensible and latent heat fluxes exist with diurnal and seasonal variations, holds. We report substantial dissimilarities between the sensible and latent heat flux transport suggesting different physical mechanisms under play, warranting further investigations. The analysis helps further our understanding of the interactions between surface spatial heterogeneity and lower atmosphere feed-backs. Measurements of flux contributions over heterogeneous landscapes have not been studied well. In particular the shifts associated with seasonal, landscape level transitions as is covered in this study. We believe that this study, by highlighting the importance of larger-scale sub-grid transport, adds a critical piece of information in assimilating and integrating observations and model outputs at multiple scales.

6 Open Research

All of the CHEESEHEAD19 observations including UWKA airborne measurements are archived at the NCAR EOL repository at `https://www.eol.ucar.edu/field_projects/cheesehead`.

The eddy4R v.0.2.0 software framework used to generate eddy-covariance flux estimates can be freely accessed at`https://github.com/NEONScience/eddy4R`. The eddy4R turbulence v0.0.16 and Environmental Response Functions v0.0.5 software modules for advanced airborne data processing were accessed under Terms of Use for this study (`https://www.eol.ucar.edu/content/cheesehead-code-policy-appendix`) and are available upon request.

Pre-processed input data for the Eddy4R flux processing routines and the calculated scale-resolved fluxes are available at the Ecometeorology lab UW server at `http://co2.aos.wisc.edu/data/CHEESEHEAD-incoming/uwka_waveletfluxes/`. The python code used to create figures for the manuscript is available at `https://github.com/sreenathpaleri/CHEESEHEAD/blob/analysis/scripts/UWKA/manuscript/plot_MS.py`

Acknowledgments
This material is based in part upon work supported by the National Science Foundation through the CHEESEHEAD19 project (grant no. AGS-1822420) and the NEON Program (grant no. DBI-0752017). The National Ecological Observatory Network is a program sponsored by the National Science Foundation and operated under cooperative agreement by Battelle. Brian Butterworth was additionally supported by the NOAA Physical Sciences Laboratory. Katrin Kohnert and Andrei Serafimovich were supported by the Helmholtz Association of German Research Centres through a Helmholtz Young Investigators Group grant (grant VH-NG-821) and by the European Union's Horizon 2020 research and innovation program under grant agreement No 72789. We also recognize that our field research occurs on the traditional territories of the Ojibwe people, which have been unjustly ceded and whose ancestors were the original scientists and naturalists who stewarded the land, air, and waters we are fortunate to observe, reflect, and hopefully help continue to flourish.

References

Amiro, B. (1998, April). Footprint climatologies for evapotranspiration in a boreal catchment. *Agricultural and Forest Meteorology*, *90*(3), 195–201. Retrieved 2022-04-12, from https://linkinghub.elsevier.com/retrieve/pii/S0168192397000968 doi: 10.1016/S0168-1923(97)00096-8

Aubinet, M., Grelle, A., Ibrom, A., Rannik, Ü., Moncrieff, J., Foken, T., ... Vesala, T. (1999). Estimates of the Annual Net Carbon and Water Exchange of Forests: The EUROFLUX Methodology. In *Advances in Ecological Research* (Vol. 30, pp. 113–175). Elsevier. Retrieved 2020-10-13, from https://linkinghub.elsevier.com/retrieve/pii/S0065250408600185 doi: 10.1016/S0065-2504(08)60018-5

Aubinet, M., Vesala, T., & Papale, D. (Eds.). (2012). *Eddy Covariance: A Practical Guide to Measurement and Data Analysis*. Dordrecht: Springer Netherlands. Retrieved 2020-10-13, from http://link.springer.com/10.1007/978-94-007-2351-1 doi: 10.1007/978-94-007-2351-1

Avissar, R., & Schmidt, T. (1998). An Evaluation of the Scale at which Ground-Surface Heat Flux Patchiness Affects the Convective Boundary Layer Using Large-Eddy Simulations. *JOURNAL OF THE ATMOSPHERIC SCIENCES*, *55*, 24.

Baldocchi, D., Falge, E., Gu, L., Olson, R., Hollinger, D., Running, S., ... Wofsy, S. (2001, November). FLUXNET: A New Tool to Study the Temporal and Spatial Variability of Ecosystem-Scale Carbon Dioxide, Water Vapor, and Energy Flux Densities. *Bulletin of the American Meteorological Society*, *82*(11), 2415 – 2434. Retrieved from https://journals.ametsoc.org/view/journals/bams/82/11/1520-0477_2001_082_2415_fantts_2_3_co_2.xml (Place: Boston MA, USA Publisher: American Meteorological Society) doi: 10.1175/1520-0477(2001)082⟨2415:FANTTS⟩2.3.CO;2

Bange, J., Beyrich, F., & Engelbart, D. A. M. (2002, December). Airborne measurements of turbulent fluxes during LITFASS-98: Comparison with ground measurements and remote sensing in a case study. *Theoretical and Applied Climatology*, *73*(1-2), 35–51. Retrieved 2021-03-01, from http://link.springer.com/10.1007/s00704-002-0692-6 doi: 10.1007/s00704-002-0692-6

Bange, J., Spieß, T., Herold, M., Beyrich, F., & Hennemuth, B. (2006, October). Turbulent fluxes from Helipod flights above quasi-homogeneous patches within the LITFASS area. *Boundary-Layer Meteorology*, *121*(1), 127–151. Retrieved 2021-01-01, from http://link.springer.com/10.1007/s10546-006-9106-0 doi: 10.1007/s10546-006-9106-0

Berger, B. W., Davis, K. J., Yi, C., Bakwin, P. S., & Zhao, C. L. (2001, April). Long-Term Carbon Dioxide Fluxes from a Very Tall Tower in a Northern Forest: Flux Measurement Methodology. *Journal of Atmospheric and Oceanic Technology*, *18*(4), 529–542. Retrieved 2022-05-12, from http://journals.ametsoc.org/doi/10.1175/1520-0426(2001)018<0529:LTCDFF>2.0.CO;2 doi: 10.1175/1520-0426(2001)018⟨0529:LTCDFF⟩2.0.CO;2

Bernhofer, C. (1992). Applying a simple three-dimensional eddy correlation system for latent and sensible heat flux to contrasting forest canopies. *Theoretical and Applied Climatology*, *46*(2-3), 163–172. Retrieved 2020-12-15, from http://link.springer.com/10.1007/BF00866096 doi: 10.1007/BF00866096

Bou-Zeid, E., Anderson, W., Katul, G. G., & Mahrt, L. (2020, July). The Persistent Challenge of Surface Heterogeneity in Boundary-Layer Meteorology: A Review. *Boundary-Layer Meteorology*. Retrieved 2020-09-30, from http://link.springer.com/10.1007/s10546-020-00551-8 doi: 10.1007/s10546-020-00551-8

Butterworth, B. J., Desai, A. R., Townsend, P. A., Petty, G. W., Andresen, C. G., Bertram, T. H., ... Wilczak, J. M. (2021). Connecting Land–Atmosphere Interactions to Surface Heterogeneity in CHEESEHEAD19. *Bulletin of the American Meteorological Society*, *102*(2), E421 – E445. Retrieved from https://journals.ametsoc.org/view/journals/bams/102/2/BAMS-D-19-0346.1.xml (Place: Boston MA, USA Publisher: American Meteorological Society) doi: 10.1175/BAMS-D-19-0346.1

Charuchittipan, D., Babel, W., Mauder, M., Leps, J.-P., & Foken, T. (2014, September). Extension of the Averaging Time in Eddy-Covariance Measurements and Its Effect on the Energy Balance Closure. *Boundary-Layer Meteorology*, *152*(3), 303–327. Retrieved 2020-10-13, from http://link.springer.com/10.1007/s10546-014-9922-6 doi: 10.1007/s10546-014-9922-6

Cuxart, J., Morales, G., Terradellas, E., & Yagüe, C. (2002, November). Study of Coherent Structures and Estimation of the Pressure Transport Terms for the Nocturnal Stable Boundary Layer. *Boundary-Layer Meteorology*, *105*(2), 305–328. Retrieved 2021-01-01, from http://link.springer.com/10.1023/A:1019974021434 doi: 10.1023/A:1019974021434

Davis, K. J., Bakwin, P. S., Yi, C., Berger, B. W., Zhao, C., Teclaw, R. M., & Isebrands, J. G. (2003). The annual cycles of CO2 and H2O exchange over a northern mixed forest as observed from a very tall tower. *Global Change Biology*, *9*(9), 1278–1293. Retrieved 2022-03-28, from http://onlinelibrary.wiley.com/doi/abs/10.1046/j.1365-2486.2003.00672.x (_eprint: https://onlinelibrary.wiley.com/doi/pdf/10.1046/j.1365-2486.2003.00672.x) doi: 10.1046/j.1365-2486.2003.00672.x

De Roo, F., & Mauder, M. (2018, April). The influence of idealized surface heterogeneity on virtual turbulent flux measurements. *Atmospheric Chemistry and Physics*, *18*(7), 5059–5074. Retrieved 2020-11-17, from https://acp.copernicus.org/articles/18/5059/2018/ doi: 10.5194/acp-18-5059-2018

Desai, A. R. (2014, February). Influence and predictive capacity of climate anomalies on daily to decadal extremes in canopy photosynthesis. *Photosynthesis Research*, *119*(1-2), 31–47. Retrieved 2022-03-28, from http://link.springer.com/10.1007/s11120-013-9925-z doi: 10.1007/s11120-013-9925-z

Desai, A. R., Khan, A. M., Zheng, T., Paleri, S., Butterworth, B., Lee, T. R., ... Metzger, S. (2021, October). Multi-Sensor Approach for High Space and Time Resolution Land Surface Temperature. *Earth and Space Science*, *8*(10). Retrieved 2022-01-24, from https://onlinelibrary.wiley.com/doi/10.1029/2021EA001842 doi: 10.1029/2021EA001842

Desai, A. R., Xu, K., Tian, H., Weishampel, P., Thom, J., Baumann, D., ... Kolka, R. (2015, February). Landscape-level terrestrial methane flux observed from a very tall tower. *Agricultural and Forest Meteorology*, *201*, 61–75. Retrieved 2022-03-28, from https://linkinghub.elsevier.com/retrieve/pii/S0168192314002688 doi: 10.1016/j.agrformet.2014.10.017

Desjardins, R. L., MacPherson, J. I., Mahrt, L., Schuepp, P., Pattey, E., Neumann, H., ... Joiner, D. W. (1997, December). Scaling up flux measurements for the boreal forest using aircraft-tower combinations. *Journal of Geophysical Research: Atmospheres*, *102*(D24), 29125–29133. Retrieved 2021-01-01, from http://doi.wiley.com/10.1029/97JD00278 doi: 10.1029/97JD00278

Drobinski, P., Brown, R. a., Flamant, P. H., & Pelon, J. (1998, September). Evidence of Organized Large Eddies by Ground-Based Doppler Lidar, Sonic Anemometer and Sodar. *Boundary-Layer Meteorology*, *88*(3), 343–361. Retrieved 2022-03-09, from http://link.springer.com/10.1023/A:1001167212584 doi: 10.1023/A:1001167212584

Eder, F., Schmidt, M., Damian, T., Träumner, K., & Mauder, M. (2015, January). Mesoscale Eddies Affect Near-Surface Turbulent Exchange: Evidence from Lidar and Tower Measurements. *Journal of Applied Meteorology and Climatology*, *54*(1), 189–206. Retrieved 2019-07-26, from http://journals.ametsoc.org/doi/10.1175/JAMC-D-14-0140.1 doi: 10.1175/JAMC-D-14-0140.1

Engelmann, C., & Bernhofer, C. (2016, October). Exploring Eddy-Covariance Measurements Using a Spatial Approach: The Eddy Matrix. *Boundary-Layer Meteorology*, *161*(1), 1–17. Retrieved 2022-03-09, from http://link.springer.com/10.1007/s10546-016-0161-x doi: 10.1007/s10546-016-0161-x

Etling, D., & Brown, R. A. (1993, August). Roll vortices in the planetary boundary layer: A review. *Boundary-Layer Meteorology*, *65*(3), 215–248. Retrieved 2019-06-26, from

http://link.springer.com/10.1007/BF00705527 doi: 10.1007/BF00705527

Finnigan, J. J., Clement, R., Malhi, Y., Leuning, R., & Cleugh, H. (2003, April). A Re-Evaluation of Long-Term Flux Measurement Techniques Part I: Averaging and Coordinate Rotation. *Boundary-Layer Meteorology*, *107*(1), 1–48. Retrieved 2020-12-10, from http://link.springer.com/10.1023/A:1021554900225 doi: 10.1023/A:1021554900225

Foken, T. (2008, September). THE ENERGY BALANCE CLOSURE PROBLEM: AN OVERVIEW. *Ecological Applications*, *18*(6), 1351–1367. Retrieved 2020-10-12, from http://doi.wiley.com/10.1890/06-0922.1 doi: 10.1890/06-0922.1

Foken, T. (2017). *Micrometeorology*. Berlin, Heidelberg: Springer Berlin Heidelberg. Retrieved 2020-10-13, from http://link.springer.com/10.1007/978-3-642-25440-6 doi: 10.1007/978-3-642-25440-6

Foken, T., Mauder, M., Liebethal, C., Wimmer, F., Beyrich, F., Leps, J.-P., ... Bange, J. (2010, July). Energy balance closure for the LITFASS-2003 experiment. *Theoretical and Applied Climatology*, *101*(1-2), 149–160. Retrieved 2020-10-12, from http://link.springer.com/10.1007/s00704-009-0216-8 doi: 10.1007/s00704-009-0216-8

Foken, T., Wimmer, F., Mauder, M., Thomas, C., & Liebethal, C. (2006). Some aspects of the energy balance closure problem. *Atmos. Chem. Phys.*, 8.

French, J., Oolman, L., & Plummer, D. (2021). *University of Wyoming King Air (UWKA) High Rate Flight Level Data. Version 1.0.* UCAR/NCAR - Earth Observing Laboratory. Retrieved 2022-03-30, from https://data.eol.ucar.edu/dataset/592.146 (Artwork Size: 24 data files, 2 ancillary/documentation files, 3 GiB Medium: NetCDF: Network Common Data Form (application/x-netcdf) Pages: 24 data files, 2 ancillary/documentation files, 3 GiB Version Number: 1.0 Type: dataset) doi: 10.26023/5B70-4VP5-XY0V

Gao, Z., Liu, H., Chen, X., Huang, M., Missik, J. E. C., Yao, J., ... Mcfarland, D. P. (2020, July). Enlarged Nonclosure of Surface Energy Balance With Increasing Atmospheric Instabilities Linked to Changes in Coherent Structures. *Journal of Geophysical Research: Atmospheres*, *125*(14). Retrieved 2020-12-12, from https://onlinelibrary.wiley.com/doi/abs/10.1029/2020JD032889 doi: 10.1029/2020JD032889

Gatz, D. F., & Smith, L. (1995, June). The standard error of a weighted mean concentration—I. Bootstrapping vs other methods. *Atmospheric Environment*, *29*(11), 1185–1193. Retrieved 2021-01-10, from https://linkinghub.elsevier.com/retrieve/pii/135223109400210C doi: 10.1016/1352-2310(94)00210-C

Haimov, S., & Rodi, A. (2013, October). Fixed-Antenna Pointing-Angle Calibration of Airborne Doppler Cloud Radar. *Journal of Atmospheric and Oceanic Technology*, *30*(10), 2320–2335. Retrieved 2022-05-12, from http://journals.ametsoc.org/doi/10.1175/JTECH-D-12-00262.1 doi: 10.1175/JTECH-D-12-00262.1

Higgins, C. W., Pardyjak, E., Froidevaux, M., Simeonov, V., & Parlange, M. B. (2013, December). Measured and Estimated Water Vapor Advection in the Atmospheric Surface Layer. *Journal of Hydrometeorology*, *14*(6), 1966–1972. Retrieved 2022-03-09, from http://journals.ametsoc.org/doi/10.1175/JHM-D-12-0166.1 doi: 10.1175/JHM-D-12-0166.1

Inagaki, A., Letzel, M. O., Raasch, S., & Kanda, M. (2006). Impact of Surface Heterogeneity on Energy Imbalance: A Study Using LES. *Journal of the Meteorological Society of Japan*, *84*(1), 187–198. Retrieved 2019-07-25, from http://joi.jlc.jst.go.jp/JST.JSTAGE/jmsj/84.187?from=CrossRef doi: 10.2151/jmsj.84.187

Kanda, M., Inagaki, A., Letzel, M. O., Raasch, S., & Watanabe, T. (2004, March). LES Study of the Energy Imbalance Problem with Eddy Covariance Fluxes. *Boundary-Layer Meteorology*, *110*(3), 381–404. Retrieved 2019-06-26, from http://link.springer.com/10.1023/B:BOUN.0000007225.45548.7a doi: 10.1023/B:BOUN.0000007225.45548.7a

Kljun, N., Calanca, P., Rotach, M. W., & Schmid, H. P. (2004, September). A Simple Parameterisation for Flux Footprint Predictions. *Boundary-Layer Meteorology*, *112*(3), 503–523. Retrieved 2021-01-01, from http://link.springer.com/10.1023/

B:BOUN.0000030653.71031.96 doi: 10.1023/B:BOUN.0000030653.71031.96

Kljun, N., Rotach, M., & Schmid, H. (2002, May). A Three-Dimensional Backward Lagrangian Footprint Model For A Wide Range Of Boundary-Layer Stratifications. *Boundary-Layer Meteorology*, *103*(2), 205–226. Retrieved 2021-01-01, from http://link.springer.com/10.1023/A:1014556300021 doi: 10.1023/A:1014556300021

Kohnert, K., Serafimovich, A., Metzger, S., Hartmann, J., & Sachs, T. (2017, December). Strong geologic methane emissions from discontinuous terrestrial permafrost in the Mackenzie Delta, Canada. *Scientific Reports*, *7*(1), 5828. Retrieved 2019-12-21, from http://www.nature.com/articles/s41598-017-05783-2 doi: 10.1038/s41598-017-05783-2

Lenschow, D. H., Mann, J., & Kristensen, L. (1994, June). How Long Is Long Enough When Measuring Fluxes and Other Turbulence Statistics? *Journal of Atmospheric and Oceanic Technology*, *11*(3), 661 – 673. Retrieved from https://journals.ametsoc.org/view/journals/atot/11/3/1520-0426_1994_011_0661_hlilew_2_0_co_2.xml (Place: Boston MA, USA Publisher: American Meteorological Society) doi: 10.1175/1520-0426(1994)011⟨0661:HLILEW⟩2.0.CO;2

Lenschow, D. H., & Stankov, B. B. (1986, June). Length Scales in the Convective Boundary Layer. *Journal of Atmospheric Sciences*, *43*(12), 1198 – 1209. Retrieved from https://journals.ametsoc.org/view/journals/atsc/43/12/1520-0469_1986_043_1198_lsitcb_2_0_co_2.xml (Place: Boston MA, USA Publisher: American Meteorological Society) doi: 10.1175/1520-0469(1986)043⟨1198:LSITCB⟩2.0.CO;2

Li, D., & Bou-Zeid, E. (2011, August). Coherent Structures and the Dissimilarity of Turbulent Transport of Momentum and Scalars in the Unstable Atmospheric Surface Layer. *Boundary-Layer Meteorology*, *140*(2), 243–262. Retrieved 2020-12-21, from http://link.springer.com/10.1007/s10546-011-9613-5 doi: 10.1007/s10546-011-9613-5

Mahrt, L. (1998). Flux Sampling Errors for Aircraft and Towers. *JOURNAL OF ATMOSPHERIC AND OCEANIC TECHNOLOGY*, *15*, 14.

Mahrt, L. (2010, April). Computing turbulent fluxes near the surface: Needed improvements. *Agricultural and Forest Meteorology*, *150*(4), 501–509. Retrieved 2020-10-12, from https://linkinghub.elsevier.com/retrieve/pii/S0168192310000389 doi: 10.1016/j.agrformet.2010.01.015

Mahrt, L., Macpherson, J. I., & Desjardins, R. (1994, February). Observations of fluxes over heterogeneous surfaces. *Boundary-Layer Meteorology*, *67*(4), 345–367. Retrieved 2019-07-25, from http://link.springer.com/10.1007/BF00705438 doi: 10.1007/BF00705438

Margairaz, F., Pardyjak, E. R., & Calaf, M. (2020, June). Surface Thermal Heterogeneities and the Atmospheric Boundary Layer: The Relevance of Dispersive Fluxes. *Boundary-Layer Meteorology*, *175*(3), 369–395. Retrieved 2020-10-13, from http://link.springer.com/10.1007/s10546-020-00509-w doi: 10.1007/s10546-020-00509-w

Maronga, B., & Raasch, S. (2013, January). Large-Eddy Simulations of Surface Heterogeneity Effects on the Convective Boundary Layer During the LITFASS-2003 Experiment. *Boundary-Layer Meteorology*, *146*(1), 17–44. Retrieved 2019-06-26, from http://link.springer.com/10.1007/s10546-012-9748-z doi: 10.1007/s10546-012-9748-z

Mauder, M., Desjardins, R. L., & MacPherson, I. (2007, July). Scale analysis of airborne flux measurements over heterogeneous terrain in a boreal ecosystem: SCALE ANALYSIS OF FLUX MEASUREMENTS. *Journal of Geophysical Research: Atmospheres*, *112*(D13), n/a–n/a. Retrieved 2019-07-25, from http://doi.wiley.com/10.1029/2006JD008133 doi: 10.1029/2006JD008133

Mauder, M., Desjardins, R. L., & MacPherson, I. (2008, December). Creating Surface Flux Maps from Airborne Measurements: Application to the Mackenzie Area GEWEX Study MAGS 1999. *Boundary-Layer Meteorology*, *129*(3), 431–450. Retrieved 2019-12-

21, from http://link.springer.com/10.1007/s10546-008-9326-6 doi: 10.1007/s10546-008-9326-6

Mauder, M., Desjardins, R. L., Pattey, E., Gao, Z., & van Haarlem, R. (2008, July). Measurement of the Sensible Eddy Heat Flux Based on Spatial Averaging of Continuous Ground-Based Observations. *Boundary-Layer Meteorology*, *128*(1), 151–172. Retrieved 2022-03-09, from http://link.springer.com/10.1007/s10546-008-9279-9 doi: 10.1007/s10546-008-9279-9

Mauder, M., Foken, T., & Cuxart, J. (2020, May). Surface-Energy-Balance Closure over Land: A Review. *Boundary-Layer Meteorology*. Retrieved 2020-06-10, from http://link.springer.com/10.1007/s10546-020-00529-6 doi: 10.1007/s10546-020-00529-6

Mauder, M., Oncley, S. P., Vogt, R., Weidinger, T., Ribeiro, L., Bernhofer, C., ... Liu, H. (2007, April). The energy balance experiment EBEX-2000. Part II: Intercomparison of eddy-covariance sensors and post-field data processing methods. *Boundary-Layer Meteorology*, *123*(1), 29–54. Retrieved 2020-11-29, from http://link.springer.com/10.1007/s10546-006-9139-4 doi: 10.1007/s10546-006-9139-4

Meijninger, W. M. L., Beyrich, F., Lüdi, A., Kohsiek, W., & Bruin, H. A. R. D. (2006, October). Scintillometer-Based Turbulent Fluxes of Sensible and Latent Heat Over a Heterogeneous Land Surface – A Contribution to Litfass-2003. *Boundary-Layer Meteorology*, *121*(1), 89–110. Retrieved 2022-02-09, from https://doi.org/10.1007/s10546-005-9022-8 doi: 10.1007/s10546-005-9022-8

Metzger, S., Durden, D., Paleri, S., Sühring, M., Butterworth, B. J., Florian, C., ... Desai, A. R. (2021, November). Novel approach to observing system simulation experiments improves information gain of surface–atmosphere field measurements. *Atmospheric Measurement Techniques*, *14*(11), 6929–6954. Retrieved 2022-01-25, from https://amt.copernicus.org/articles/14/6929/2021/ doi: 10.5194/amt-14-6929-2021

Metzger, S., Durden, D., Sturtevant, C., Luo, H., Pingintha-Durden, N., Sachs, T., ... Desai, A. R. (2017, August). eddy4R 0.2.0: a DevOps model for community-extensible processing and analysis of eddy-covariance data based on R, Git, Docker, and HDF5. *Geoscientific Model Development*, *10*(9), 3189–3206. Retrieved 2019-11-07, from https://www.geosci-model-dev.net/10/3189/2017/ doi: 10.5194/gmd-10-3189-2017

Metzger, S., Junkermann, W., Mauder, M., Butterbach-Bahl, K., Trancón y Widemann, B., Neidl, F., ... Foken, T. (2013, April). Spatially explicit regionalization of airborne flux measurements using environmental response functions. *Biogeosciences*, *10*(4), 2193–2217. Retrieved 2019-12-20, from https://www.biogeosciences.net/10/2193/2013/ doi: 10.5194/bg-10-2193-2013

Morrison, T., Calaf, M., Higgins, C. W., Drake, S. A., Perelet, A., & Pardyjak, E. (2021, August). The Impact of Surface Temperature Heterogeneity on Near-Surface Heat Transport. *Boundary-Layer Meteorology*, *180*(2), 247–272. Retrieved 2022-03-09, from https://link.springer.com/10.1007/s10546-021-00624-2 doi: 10.1007/s10546-021-00624-2

Nordbo, A., & Katul, G. (2013, January). A Wavelet-Based Correction Method for Eddy-Covariance High-Frequency Losses in Scalar Concentration Measurements. *Boundary-Layer Meteorology*, *146*(1), 81–102. Retrieved 2019-12-21, from http://link.springer.com/10.1007/s10546-012-9759-9 doi: 10.1007/s10546-012-9759-9

Oncley, S. P., Foken, T., Vogt, R., Kohsiek, W., DeBruin, H. A. R., Bernhofer, C., ... Weidinger, T. (2007, March). The Energy Balance Experiment EBEX-2000. Part I: overview and energy balance. *Boundary-Layer Meteorology*, *123*(1), 1–28. Retrieved 2020-11-29, from http://link.springer.com/10.1007/s10546-007-9161-1 doi: 10.1007/s10546-007-9161-1

Pielke, R. A., Sr, ., Avissar, R., Raupach, M., Dolman, A. J., Zeng, X., & Denning, A. S. (1998). Interactions between the atmosphere and terrestrial ecosystems: influence on weather and climate. *Global Change Biology*, *4*(5), 461–475. Retrieved from https://onlinelibrary.wiley.com/doi/abs/10.1046/j.1365-2486.1998.t01-1-00176.x

(_eprint: https://onlinelibrary.wiley.com/doi/pdf/10.1046/j.1365-2486.1998.t01-1-00176.x) doi: https://doi.org/10.1046/j.1365-2486.1998.t01-1-00176.x

Rodi, A. (2011). King of the air: The evolution and capabilities of wyoming's observation aircraft. *Meteorological Technology International*, 44–47.

Rodi, A. R., & Leon, D. C. (2012). Correction of static pressure on a research aircraft in accelerated flight using differential pressure measurements. *Atmospheric Measurement Techniques*, *5*(11), 2569–2579. Retrieved from https://amt.copernicus.org/articles/5/2569/2012/ doi: 10.5194/amt-5-2569-2012

Rodi, A. R., & Spyers-Duran, P. A. (1972). Analysis of Time Response of Airborne Temperature Sensors. *Journal of Applied Meteorology and Climatology*, *11*(3), 554 – 556. Retrieved from https://journals.ametsoc.org/view/journals/apme/11/3/1520-0450_1972_011_0554_aotroa_2_0_co_2.xml (Place: Boston MA, USA Publisher: American Meteorological Society) doi: 10.1175/1520-0450(1972)011⟨0554:AOTROA⟩2.0.CO;2

Salesky, S., & Anderson, W. (2020, September). Coherent Structures Modulate Atmospheric Surface Layer Flux-Gradient Relationships. *Physical Review Letters*, *125*(12), 124501. Retrieved 2020-10-20, from https://link.aps.org/doi/10.1103/PhysRevLett.125.124501 doi: 10.1103/PhysRevLett.125.124501

Salesky, S. T., Chamecki, M., & Bou-Zeid, E. (2017, April). On the Nature of the Transition Between Roll and Cellular Organization in the Convective Boundary Layer. *Boundary-Layer Meteorology*, *163*(1), 41–68. Retrieved 2020-12-21, from http://link.springer.com/10.1007/s10546-016-0220-3 doi: 10.1007/s10546-016-0220-3

Steinfeld, G., Letzel, M. O., Raasch, S., Kanda, M., & Inagaki, A. (2007, March). Spatial representativeness of single tower measurements and the imbalance problem with eddy-covariance fluxes: results of a large-eddy simulation study. *Boundary-Layer Meteorology*, *123*(1), 77–98. Retrieved 2019-06-26, from http://link.springer.com/10.1007/s10546-006-9133-x doi: 10.1007/s10546-006-9133-x

Stoy, P. C., Mauder, M., Foken, T., Marcolla, B., Boegh, E., Ibrom, A., ... Varlagin, A. (2013, April). A data-driven analysis of energy balance closure across FLUXNET research sites: The role of landscape scale heterogeneity. *Agricultural and Forest Meteorology*, *171-172*, 137–152. Retrieved 2019-12-19, from https://linkinghub.elsevier.com/retrieve/pii/S0168192312003413 doi: 10.1016/j.agrformet.2012.11.004

Strunin, M. A., & Hiyama, T. (2004, November). Applying wavelet transforms to analyse aircraft-measured turbulence and turbulent fluxes in the atmospheric boundary layer over eastern Siberia. *Hydrological Processes*, *18*(16), 3081–3098. Retrieved 2019-07-26, from http://doi.wiley.com/10.1002/hyp.5750 doi: 10.1002/hyp.5750

Strunin, M. A., & Hiyama, T. (2005, December). Spectral Structure of Small-Scale Turbulent and Mesoscale Fluxes in the Atmospheric Boundary Layer over a Thermally Inhomogeneous Land Surface. *Boundary-Layer Meteorology*, *117*(3), 479–510. Retrieved 2019-07-26, from http://link.springer.com/10.1007/s10546-005-2188-2 doi: 10.1007/s10546-005-2188-2

Strunin, M. A., Hiyama, T., Asanuma, J., & Ohata, T. (2004, June). Aircraft Observations of the Development of Thermal Internal Boundary Layers and Scaling of the Convective Boundary Layer Over Non-Homogeneous Land Surfaces. *Boundary-Layer Meteorology*, *111*(3), 491–522. Retrieved 2019-07-11, from http://link.springer.com/10.1023/B:BOUN.0000016542.72958.e9 doi: 10.1023/B:BOUN.0000016542.72958.e9

Stull, R. B. (1988). An Introduction to Boundary Layer Meteorology. In R. B. Stull (Ed.), *An Introduction to Boundary Layer Meteorology* (pp. 1–27). Dordrecht: Springer Netherlands. Retrieved 2021-01-01, from http://link.springer.com/10.1007/978-94-009-3027-8_1 doi: 10.1007/978-94-009-3027-8_1

Sun, J., Desjardins, R., Mahrt, L., & MacPherson, I. (1998, October). Transport of carbon dioxide, water vapor, and ozone by turbulence and local circulations. *Journal of Geophysical Research: Atmospheres*, *103*(D20), 25873–25885. Retrieved 2020-10-13, from http://doi.wiley.com/10.1029/98JD02439 doi: 10.1029/98JD02439

Torrence, C., & Compo, G. P. (1998). A Practical Guide to Wavelet Analysis. *Bulletin of the American Meteorological Society*, *79*(1), 18.

Wang, Z., French, J., Vali, G., Wechsler, P., Haimov, S., Rodi, A., ... Pazmany, A. L. (2012, May). Single Aircraft Integration of Remote Sensing and In Situ Sampling for the Study of Cloud Microphysics and Dynamics. *Bulletin of the American Meteorological Society*, *93*(5), 653–668. Retrieved 2022-04-12, from https://journals.ametsoc.org/doi/10.1175/BAMS-D-11-00044.1 doi: 10.1175/BAMS-D-11-00044.1

Wulfmeyer, V., Turner, D. D., Baker, B., Banta, R., Behrendt, A., Bonin, T., ... Weckwerth, T. (2018, August). A New Research Approach for Observing and Characterizing Land–Atmosphere Feedback. *Bulletin of the American Meteorological Society*, *99*(8), 1639–1667. Retrieved 2019-12-24, from http://journals.ametsoc.org/doi/10.1175/BAMS-D-17-0009.1 doi: 10.1175/BAMS-D-17-0009.1

Xu, F., Wang, W., Wang, J., Xu, Z., Qi, Y., & Wu, Y. (2017, August). Area-averaged evapotranspiration over a heterogeneous land surface: aggregation of multi-point EC flux measurements with a high-resolution land-cover map and footprint analysis. *Hydrology and Earth System Sciences*, *21*(8), 4037–4051. Retrieved 2020-10-12, from https://hess.copernicus.org/articles/21/4037/2017/ doi: 10.5194/hess-21-4037-2017

Xu, K., Sühring, M., Metzger, S., Durden, D., & Desai, A. R. (2020, April). Can Data Mining Help Eddy Covariance See the Landscape? A Large-Eddy Simulation Study. *Boundary-Layer Meteorology*. Retrieved 2020-05-08, from http://link.springer.com/10.1007/s10546-020-00513-0 doi: 10.1007/s10546-020-00513-0

Zhang, G., Leclerc, M. Y., Duarte, H. F., Durden, D., Werth, D., Kurzeja, R., & Parker, M. (2014, March). Multi-scale decomposition of turbulent fluxes above a forest canopy. *Agricultural and Forest Meteorology*, *186*, 48–63. Retrieved 2021-01-20, from https://linkinghub.elsevier.com/retrieve/pii/S0168192313003006 doi: 10.1016/j.agrformet.2013.11.010

Zhang, Y., Liu, H., Foken, T., Williams, Q. L., Liu, S., Mauder, M., & Liebethal, C. (2010, August). Turbulence Spectra and Cospectra Under the Influence of Large Eddies in the Energy Balance EXperiment (EBEX). *Boundary-Layer Meteorology*, *136*(2), 235–251. Retrieved 2020-10-13, from http://link.springer.com/10.1007/s10546-010-9504-1 doi: 10.1007/s10546-010-9504-1

Zhou, Y., Li, D., & Li, X. (2019, August). The Effects of Surface Heterogeneity Scale on the Flux Imbalance under Free Convection. *Journal of Geophysical Research: Atmospheres*, 2018JD029550. Retrieved 2019-12-19, from https://onlinelibrary.wiley.com/doi/abs/10.1029/2018JD029550 doi: 10.1029/2018JD029550

Supporting Information for "Space - scale resolved surface-atmospheric fluxes across a heterogeneous mid-latitude forested landscape"

Sreenath Paleri [1], Ankur R. Desai [1], Stefan Metzger [2,1], David Durden [2], Brian J. Butterworth [3,4], Matthias Mauder [5,6], Katrin Kohnert [7] *, Andrei Serafimovich [7] †

[1]Department of Atmospheric and Oceanic Sciences, University of Wisconsin-Madison, Madison, Wisconsin, USA

[2]Battelle, National Ecological Observatory Network, 1685 38th Street, Boulder, Colorado, USA

[3]Cooperative Institute for Research in Environmental Sciences, University of Colorado, Boulder, Colorado, USA

[4]NOAA Physical Sciences Laboratory, Boulder, Colorado, USA

[5]Institute of Hydrology and Meteorology, Technische Universität Dresden, Dresden, Germany

[6]Institute of Meteorology and Climate Research – Atmospheric Environmental Research, Karlsruhe Institute of Technology, Garmisch-Partenkirchen, Germany

[7] GFZ German Research Centre for Geosciences, Telegrafenberg, Potsdam, Germany

Corresponding author: Sreenath Paleri, Dept of Atmospheric and Oceanic Sciences, University of Wisconsin-Madison, Madison, WI 53706, USA. (paleri@wisc.edu)

*Now at: German Council of Experts on Climate Change, Berlin, Germany

†Now at: Deutscher Wetterdienst, Offenbach, Germany

May 18, 2022, 8:08pm

Contents of this file

1. Table S1

2. Figures S1 to S18

Table S1. IOP averaged scale-resolved heat fluxes. RMS error values scaled by $\sqrt{N_{samples}}$

IOP	Total LE	Total H	Turb. LE	Meso. LE	Turb. H	Meso. H
July	179.98 ± 4.78	88.31 ± 0.94	123.07 ± 2.40	56.92 ± 4.14	71.25 ± 0.74	17.05 ± 0.58
Aug.	256.44 ±2.92	88.04 ± 1.02	210.28 ± 2.38	46.16 ± 1.69	68.02 ± 0.78	20.01 ± 0.66
Sep.	69.01 ± 2.86	89.13 ± 1.13	49.36 ± 1.87	19.65 ± 2.17	76.36 ± 0.78	12.77 ± 0.81

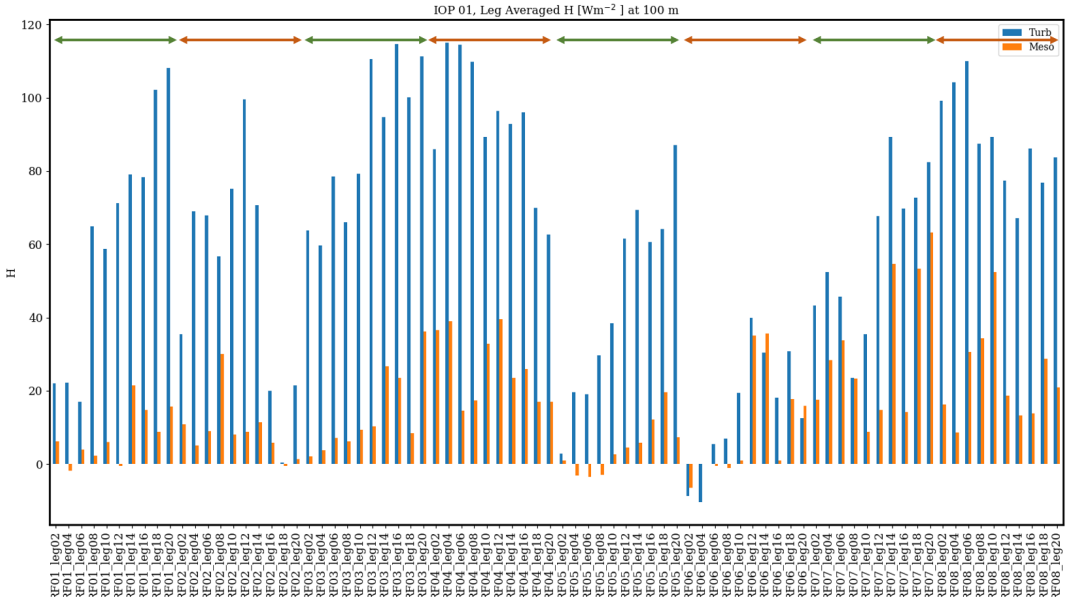

Figure S1. Flight leg averaged, scale-resolved sensible heat fluxes at 100m for the July IOP. x axis shows flight leg names. Arrows at the top of the figure span the length of one research flight. Green arrows cover morning flights and orange arrows cover afternoon flights.

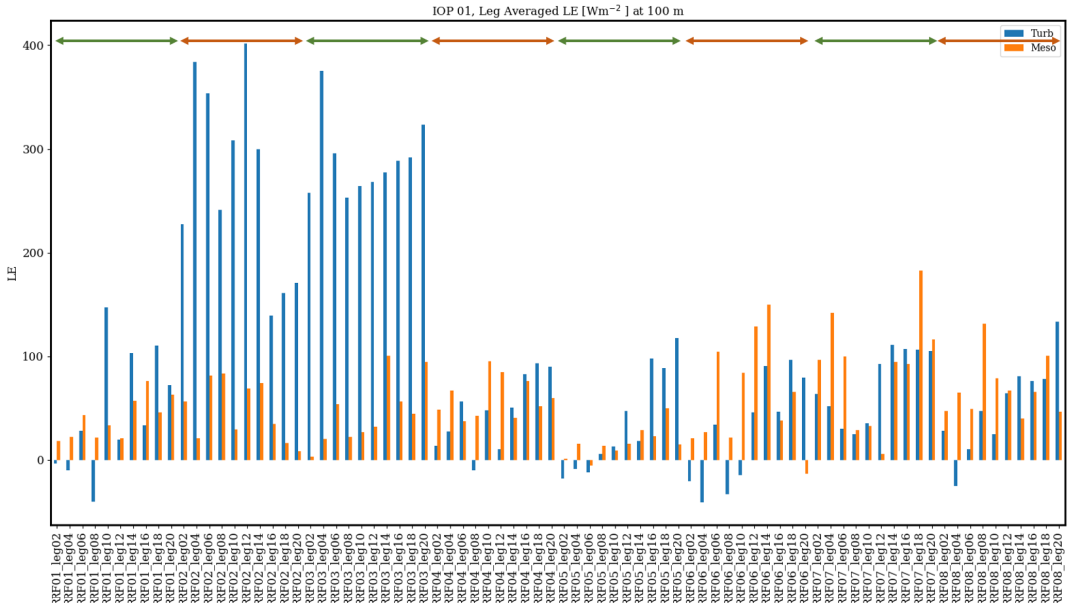

Figure S2. Flight leg averaged, scale-resolved latent heat fluxes at 100m for the July IOP. x axis shows flight leg names. Arrows at the top of the figure span the length of one research flight. Green arrows cover morning flights and orange arrows cover afternoon flights.

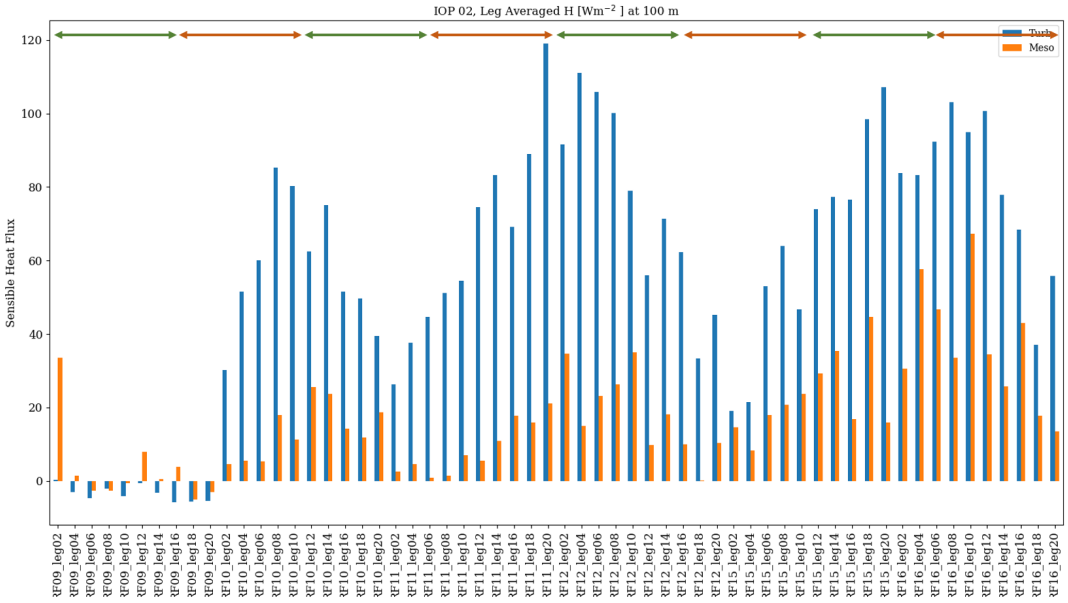

Figure S3. Flight leg averaged, scale-resolved sensible heat fluxes at 100m for the August IOP. x axis shows flight leg names. Arrows at the top of the figure span the length of one research flight. Green arrows cover morning flights and orange arrows cover afternoon flights.

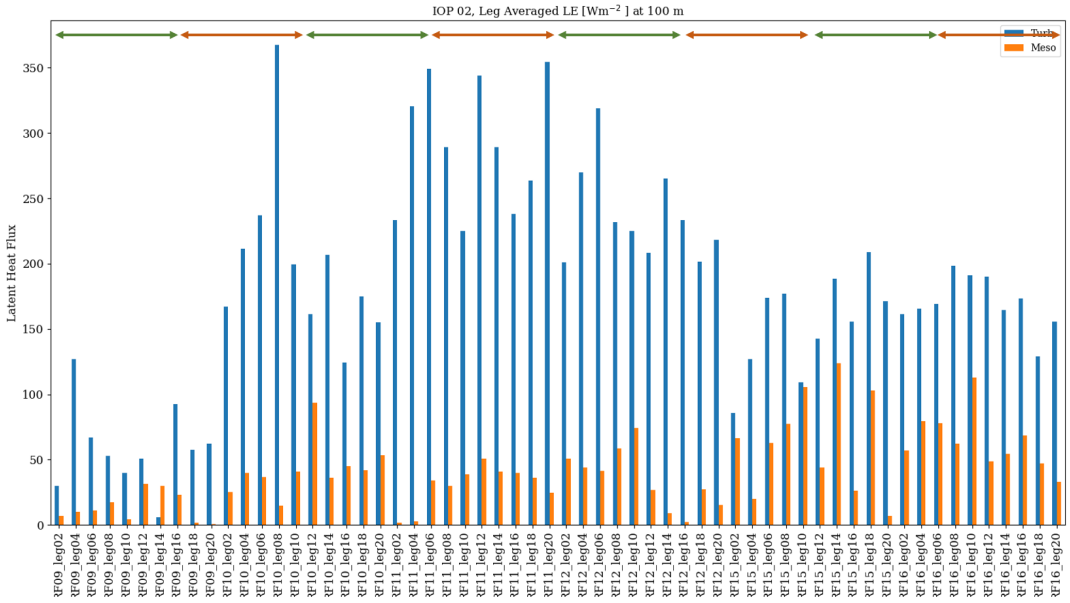

Figure S4. Flight leg averaged, scale-resolved latent heat fluxes at 100m for the August IOP. x axis shows flight leg names. Arrows at the top of the figure span the length of one research flight. Green arrows cover morning flights and orange arrows cover afternoon flights.

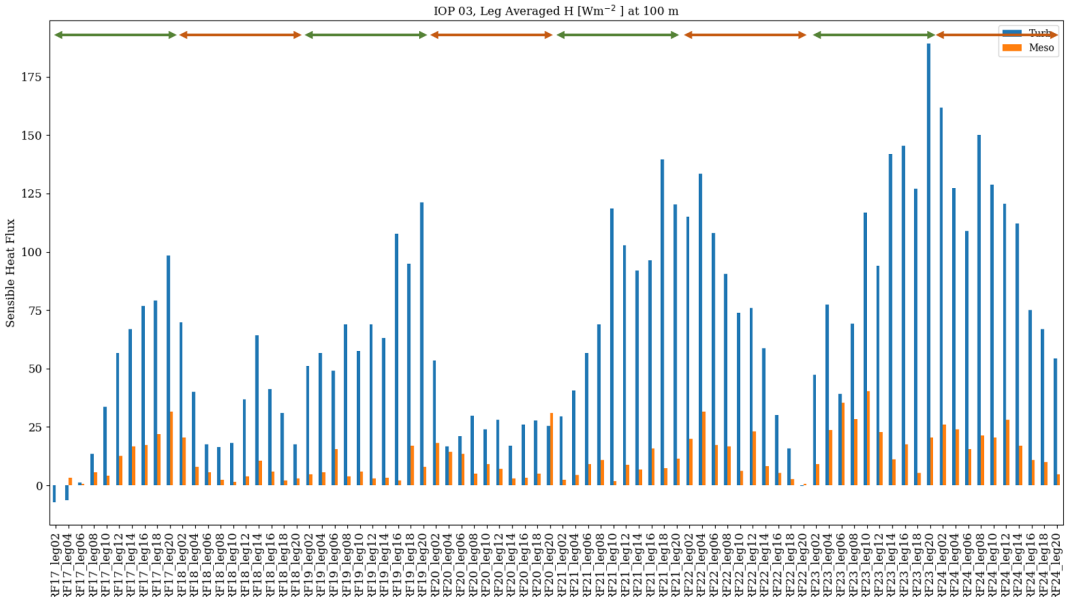

Figure S5. Flight leg averaged, scale-resolved sensible heat fluxes at 100m for the September IOP. x axis shows flight leg names. Arrows at the top of the figure span the length of one research flight. Green arrows cover morning flights and orange arrows cover afternoon flights.

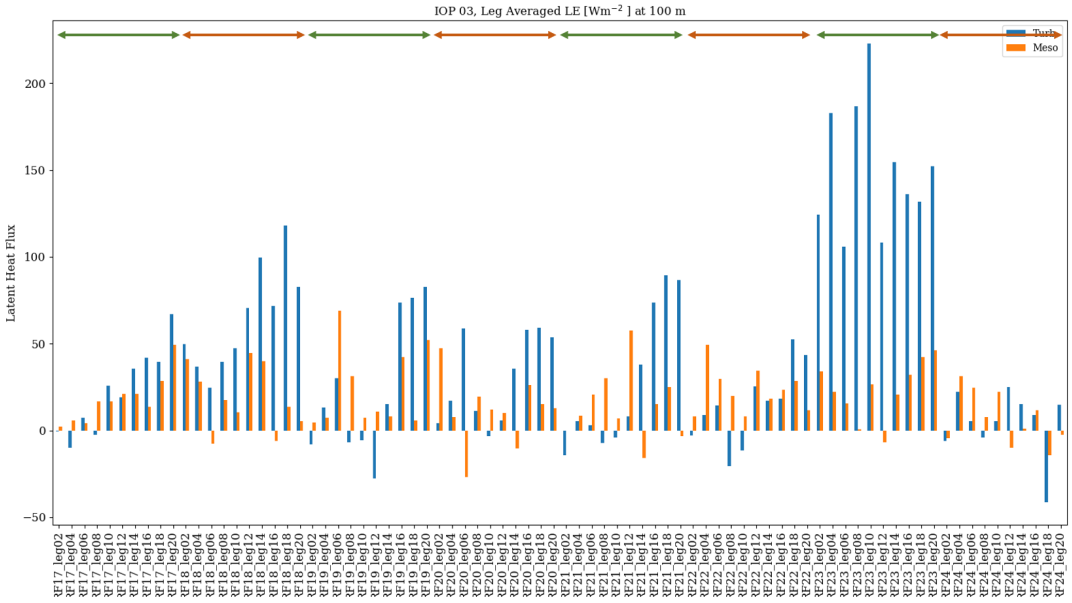

Figure S6. Flight leg averaged, scale-resolved latent heat fluxes at 100m for the September IOP. x axis shows flight leg names. Arrows at the top of the figure span the length of one research flight. Green arrows cover morning flights and orange arrows cover afternoon flights.

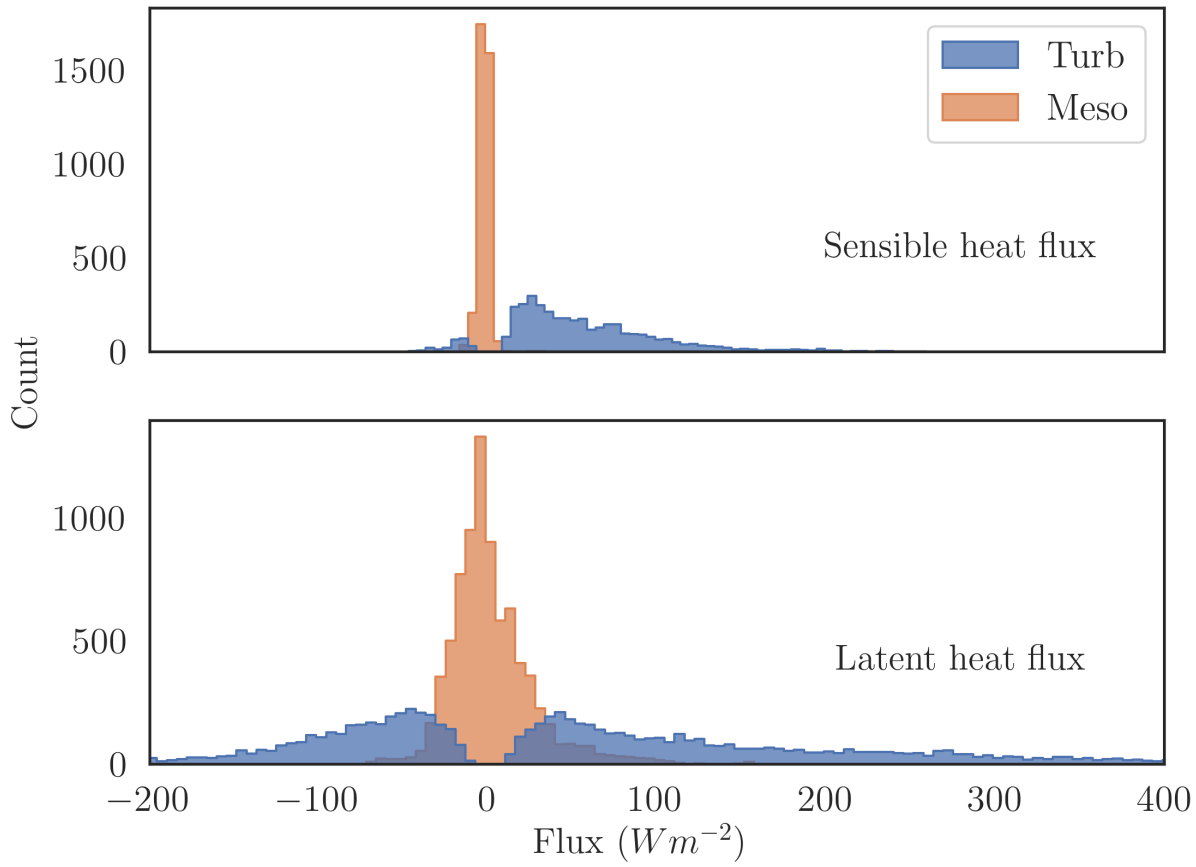

Figure S7. Histograms of turbulent and mesoscale fluxes for cases when the measured mesoscale fractions are lesser than 0

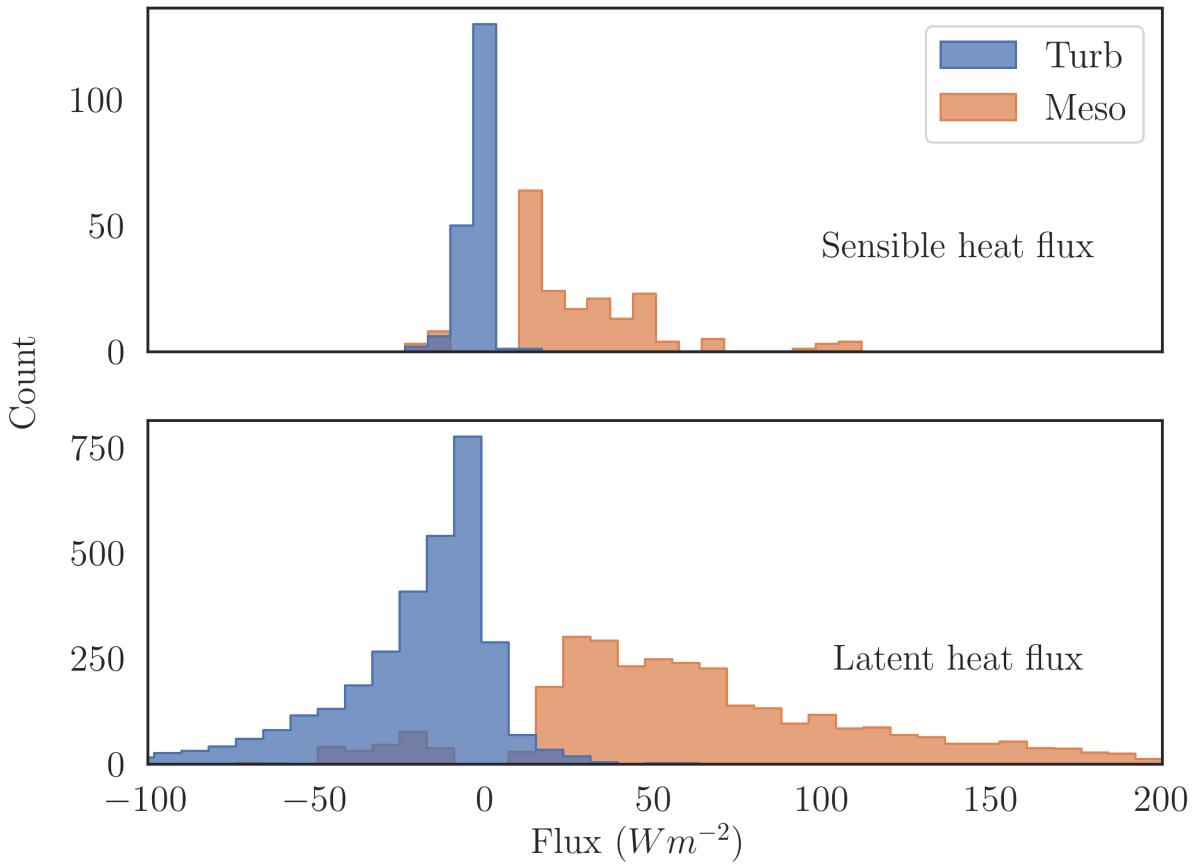

Figure S8. Histograms of turbulent and mesoscale fluxes for cases when the measured mesoscale fractions are greater than 1

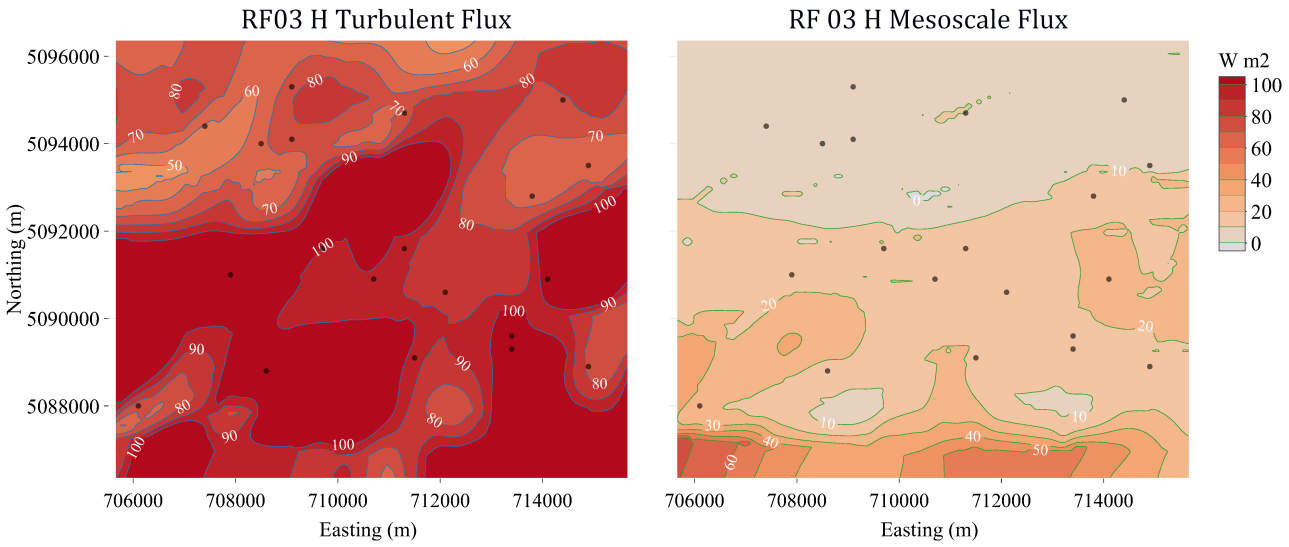

Figure S9. Turbulent (left) and mesoscale (right) sensible heat flux topographies for Research Flight 03 in the July IOP, 11 Jul. 09:20 to 11:20 CDT, over the 10x10 km CHEESEHEAD core domain. The brown dots are the NCAR-ISFS tower locations.

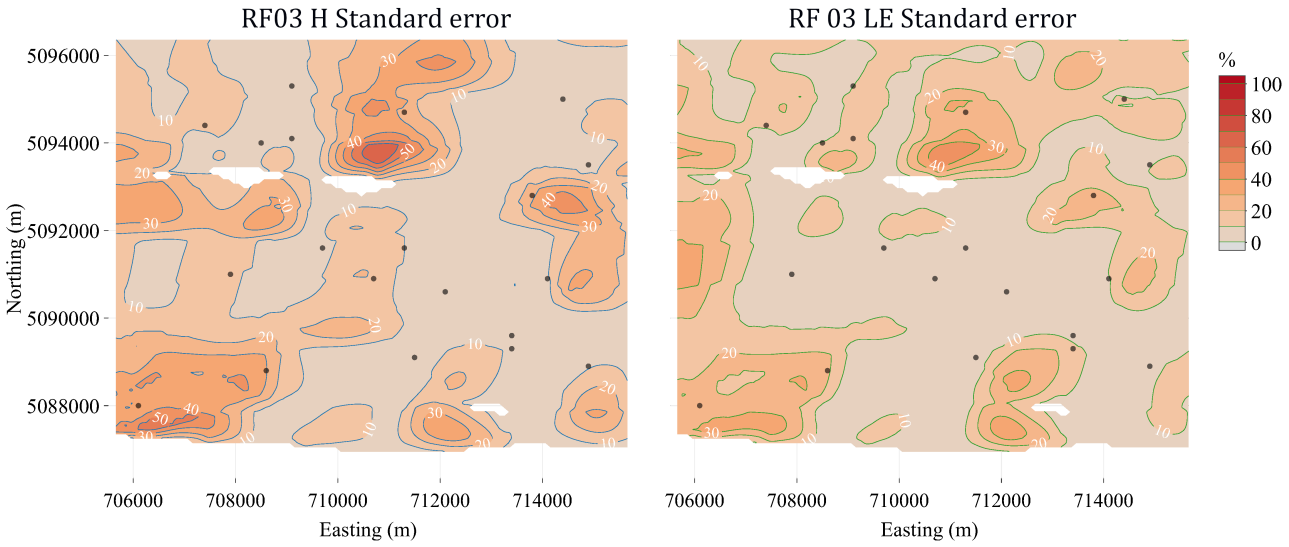

Figure S10. Standard error topographies for sensible (left) and latent (right) heat fluxes for Research Flight 03 in the July IOP, 11 Jul. 09:20 to 11:20 CDT, over the 10x10 km CHEESE-HEAD core domain. The brown dots are the NCAR-ISFS tower locations.

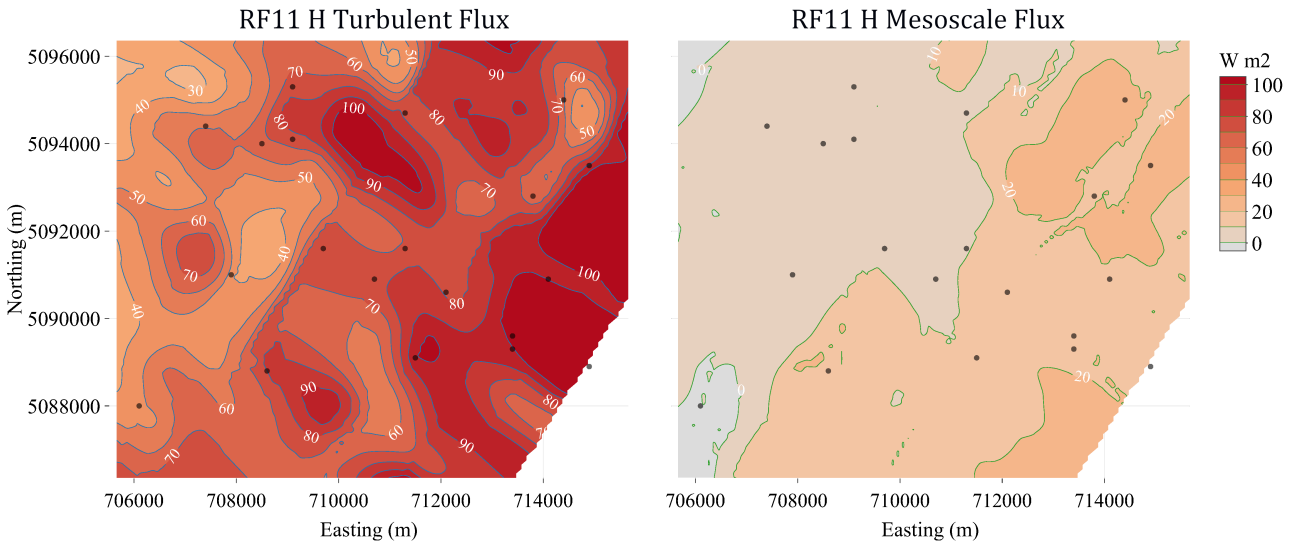

Figure S11. Turbulent (left) and mesoscale (right) sensible heat flux topographies for Research Flight 11 in the August IOP, 21 Aug. 09:00 to 11:30 CDT, over the 10x10 km CHEESEHEAD core domain. The brown dots are the NCAR-ISFS tower locations.

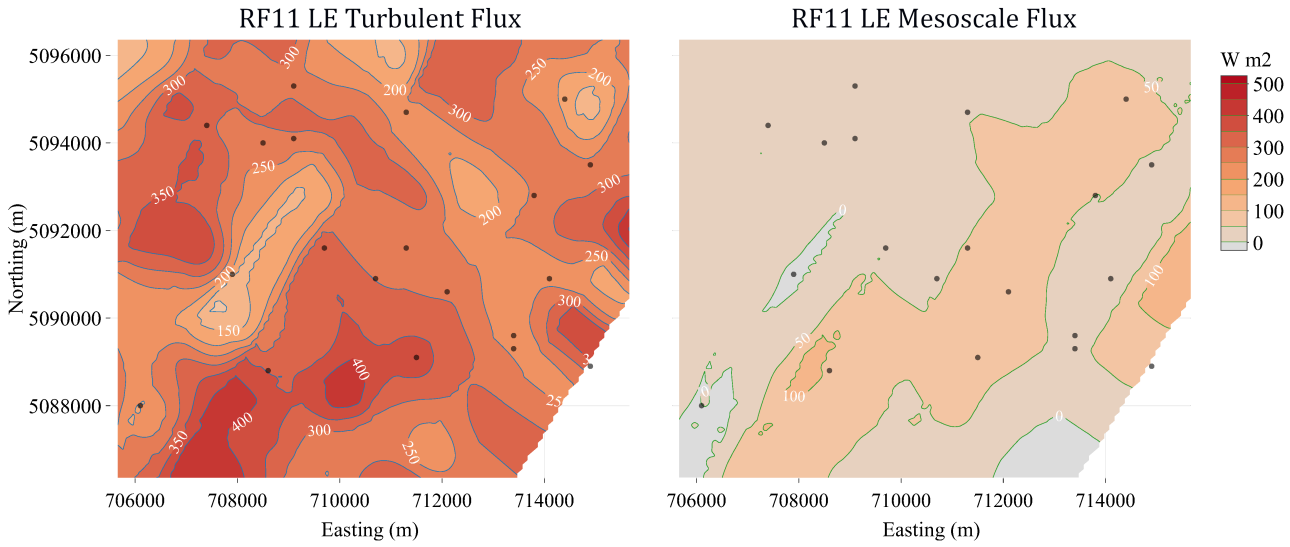

Figure S12. Turbulent (left) and mesoscale (right) latent heat flux topographies for Research Flight 11 in the August IOP, 21 Aug. 09:00 to 11:30 CDT, over the 10x10 km CHEESEHEAD core domain. The brown dots are the NCAR-ISFS tower locations.

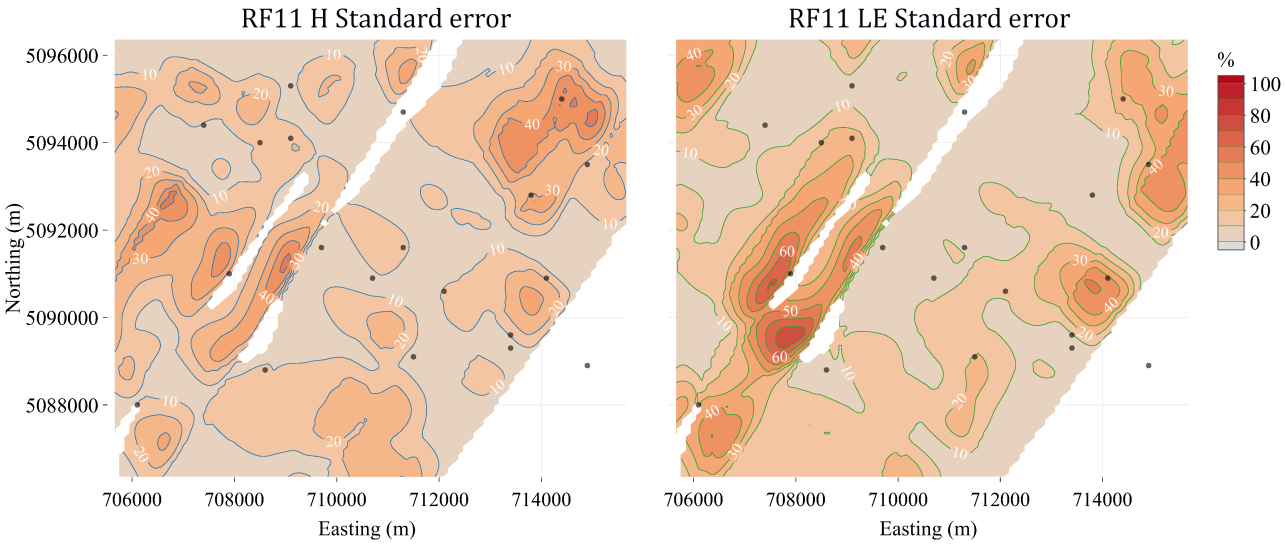

Figure S13. Standard error topographies for sensible (left) and latent (right) heat fluxes for Research Flight 11 in the August IOP, 21 Aug. 09:00 to 11:30 CDT, over the 10x10 km CHEESEHEAD core domain. The brown dots are the NCAR-ISFS tower locations.

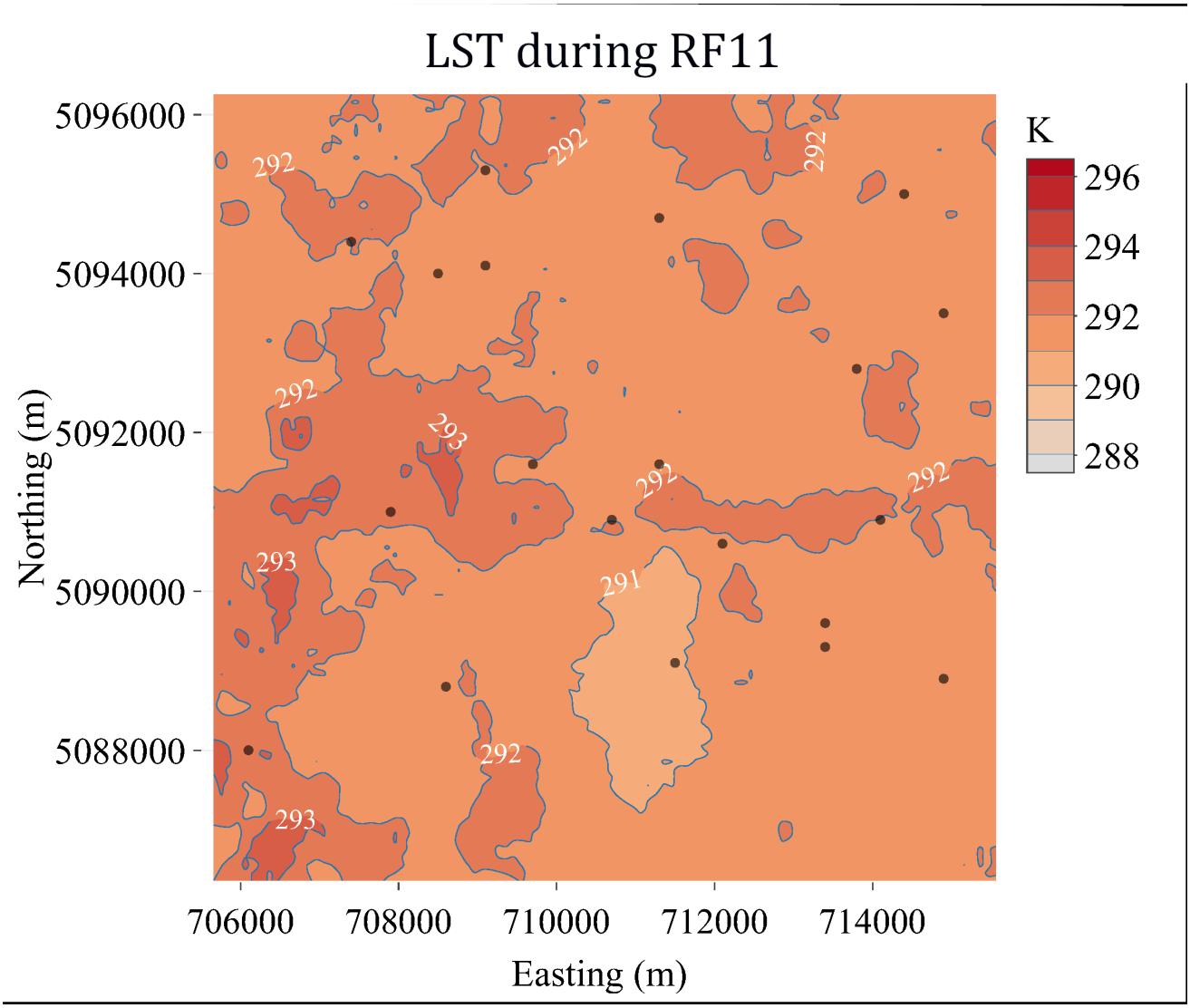

Figure S14. Fusion Land Surface Temperature data for the 10x10 km domain during Research Flight 11, 21 Aug. 2019 09:00 to 11:30 CDT , from Desai et al. (2021)

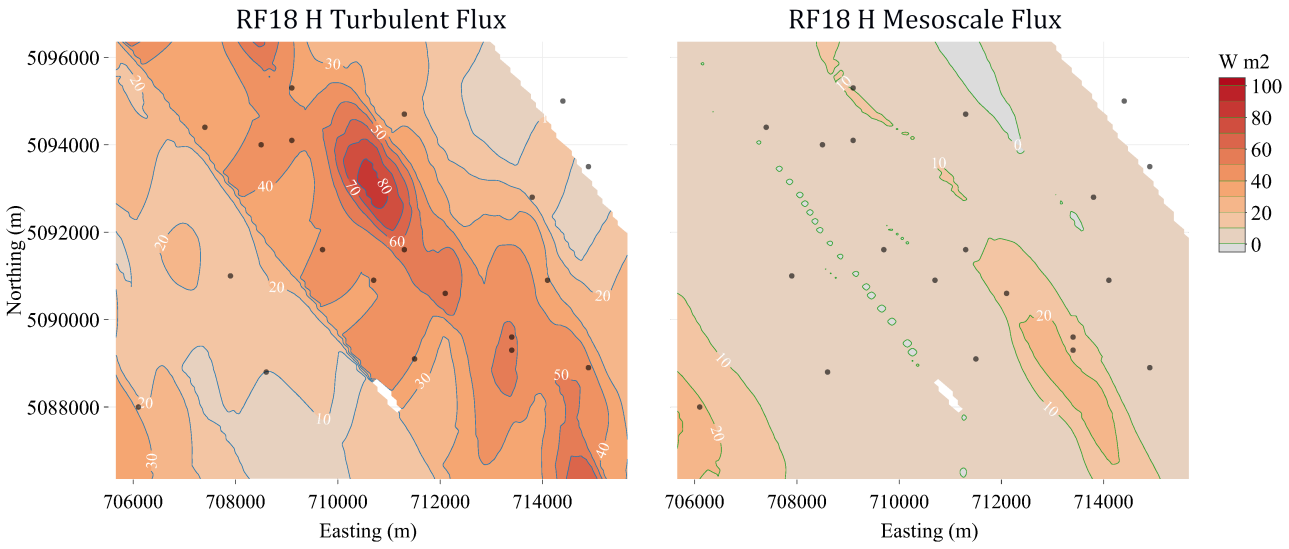

Figure S15. Turbulent (left) and mesoscale (right) sensible heat flux topographies for Research Flight 18 in the September IOP, 24 Sep. 14:00 to 16:30 CDT, over the 10x10 km CHEESEHEAD core domain. The brown dots are the NCAR-ISFS tower locations.

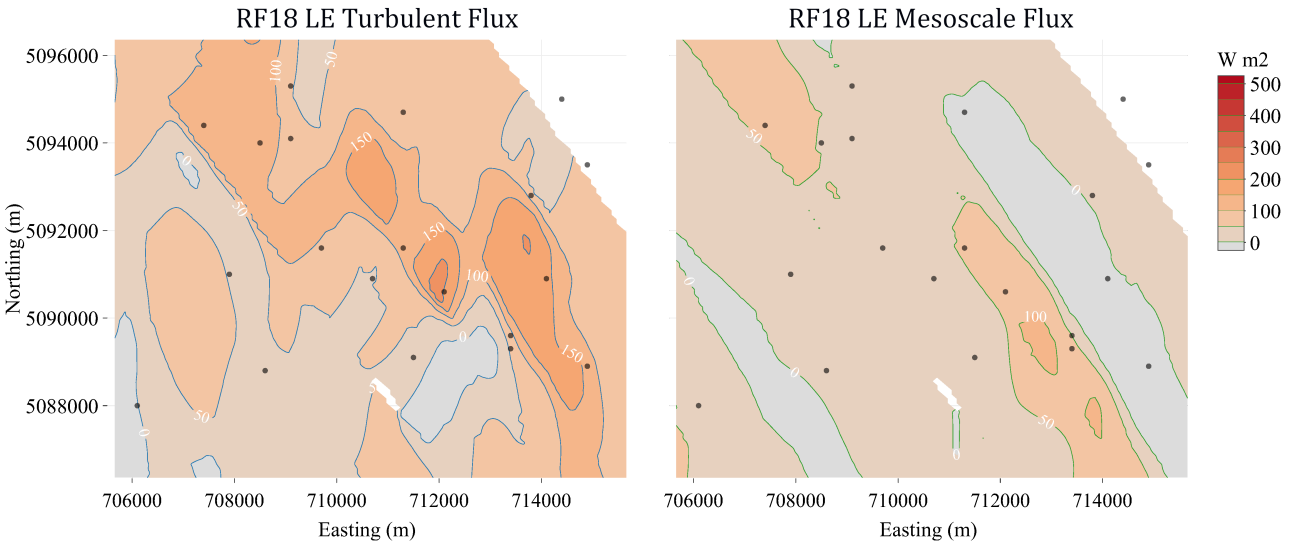

Figure S16. Turbulent (left) and mesoscale (right) latent heat flux topographies for Research Flight 18 in the September IOP, 24 Sep. 14:00 to 16:30 CDT, over the 10x10 km CHEESEHEAD core domain. The brown dots are the NCAR-ISFS tower locations.

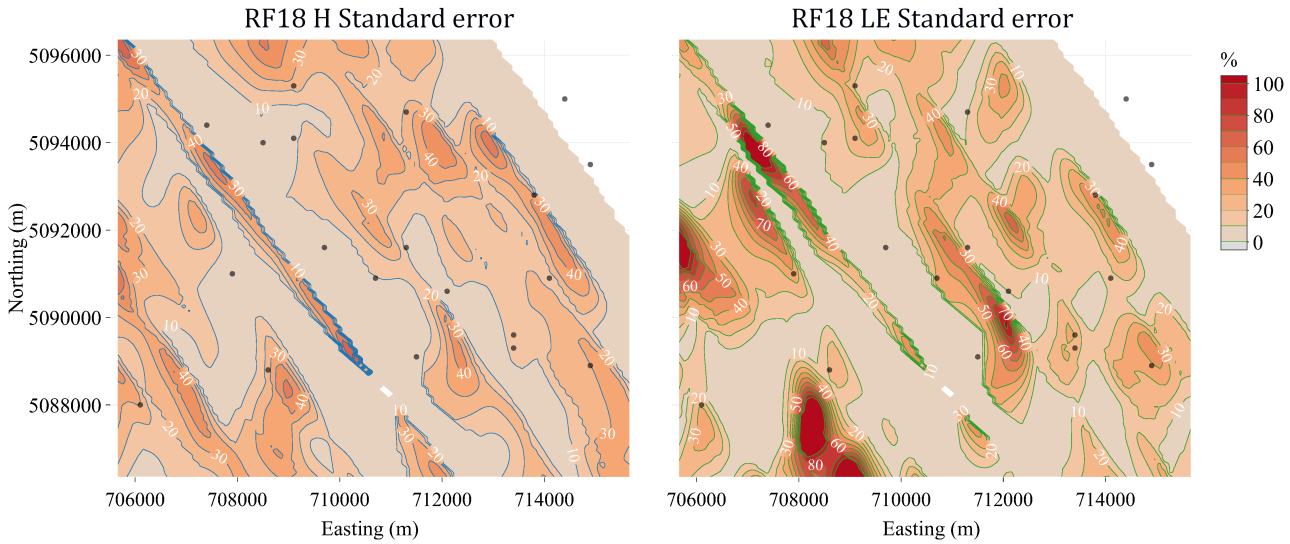

Figure S17. Standard error topographies for sensible (left) and latent (right) heat fluxes for Research Flight 18 in the September IOP, 24 Sep. 14:00 to 16:30 CDT, over the 10x10 km CHEESEHEAD core domain. The brown dots are the NCAR-ISFS tower locations.

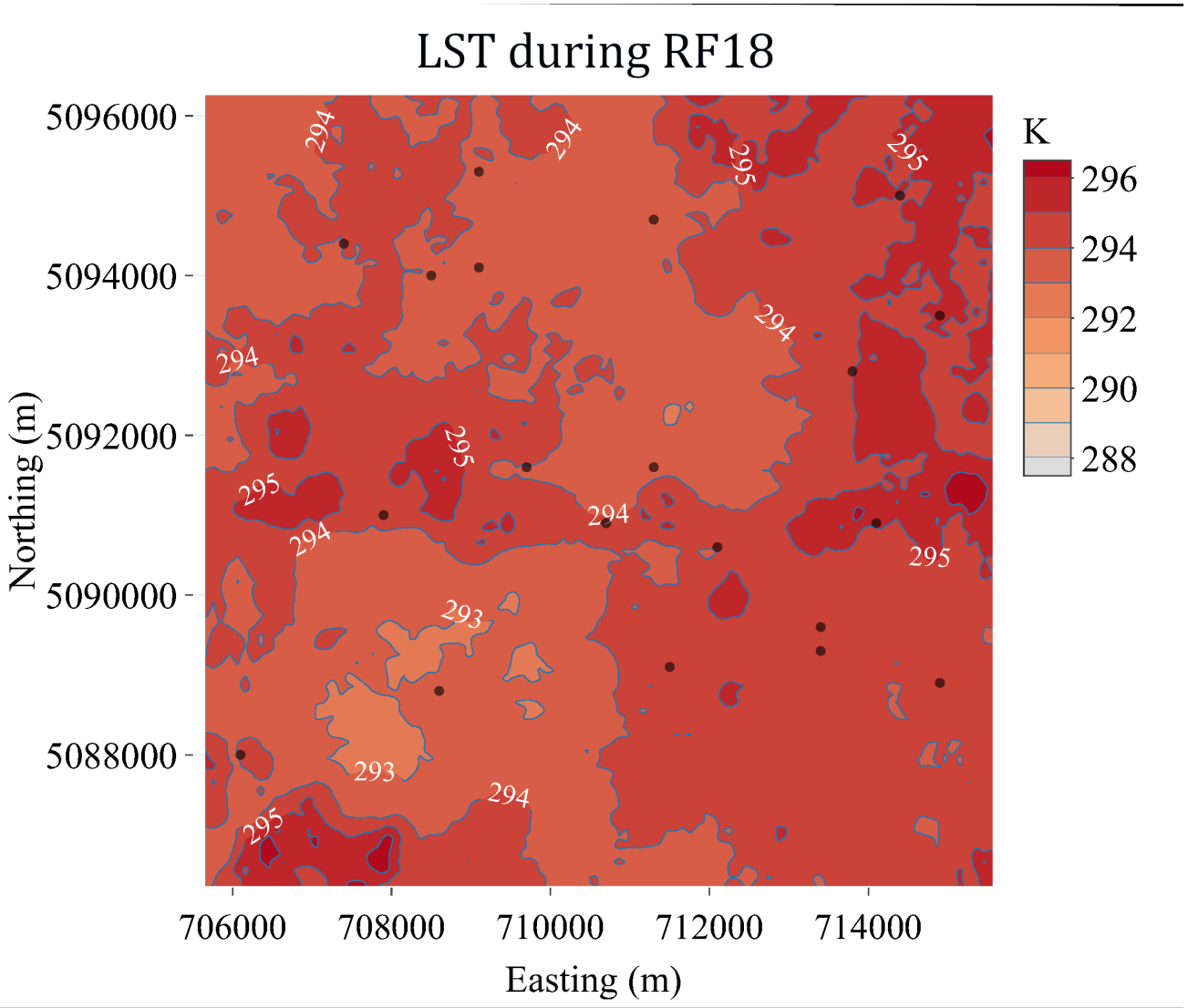

Figure S18. Fusion Land Surface Temperature data for the 10x10 km domain during Research Flight 18 in the September IOP, 24 Sep. 14:00 to 16:30 CDT, from Desai et al. (2021)